Inclusive $D^{*\pm}$ production in $p\bar{p}$ collisions with massive charm quarks

B. A. Kniehl, G. Kramer, and I. Schienbein
II. Institut für Theoretische Physik, Universität Hamburg, Luruper Chaussee 149, 22761 Hamburg, Germany

H. Spiesberger
Institut für Physik, Johannes-Gutenberg-Universität, Staudinger Weg 7, 55099 Mainz, Germany
(Received 21 October 2004; published 20 January 2005)

We calculate the next-to-leading-order cross section for the inclusive production of $D^{*\pm}$ mesons in $p\bar{p}$ collisions as a function of the transverse momentum and the rapidity in two approaches using massive or massless charm quarks. For the inclusive cross section, we derive the massless limit from the massive theory. We find that this limit differs from the genuine massless version with $\overline{\mathrm{MS}}$ (minimal-subtraction) factorization by finite corrections. By adjusting subtraction terms, we establish a massive theory with $\overline{\mathrm{MS}}$ subtraction which approaches the massless theory with increasing transverse momentum. With these results and including the contributions due to the charm and anticharm content of the proton and antiproton, we calculate the inclusive $D^{*\pm}$ cross section in $p\bar{p}$ collisions using realistic evolved nonperturbative fragmentation functions and compare with recent data from the CDF Collaboration at the Fermilab Tevatron at center-of-mass energy $\sqrt{S} = 1.96$ TeV. We find reasonable, though not perfect, agreement with the measured cross sections.

DOI: 10.1103/PhysRevD.71.014018 PACS numbers: 12.38.Bx, 12.39.St, 13.85.Ni, 14.40.Lb

I. INTRODUCTION

Recently, there has been quite some interest in the study of charm production in proton-antiproton collisions at high energies, both experimentally and theoretically. The CDF Collaboration at the Fermilab Tevatron presented results for prompt charm meson production cross sections at center-of-mass energy $\sqrt{S} = 1.96$ TeV. The differential cross section $d\sigma/dp_T$ was measured as a function of transverse momentum (p_T) in the central rapidity (y) region $|y| \leq 1$ for inclusive production of D^0, D^+, D^{*+} and D_s^+ mesons and their charge conjugates [1]. For definiteness, we shall concentrate here on $D^{*\pm}$ mesons. However, our results readily carry over to any other heavy-flavored hadrons.

On the theoretical side, various approaches for next-to-leading-order (NLO) calculations in perturbative QCD have been applied for comparison with experimental data. In the so-called massless scheme [2,3], also known as zero-mass variable-flavor-number (ZM-VFN) scheme, which is the conventional parton model approach implemented in the modified minimal-subtraction ($\overline{\mathrm{MS}}$) scheme, the zero-mass parton approximation is applied also to the charm quark, although its mass m is certainly much larger than the asymptotic scale parameter Λ_{QCD}. In this approach, the charm quark is also an incoming parton originating from the proton or antiproton, leading to additional contributions, besides those from the gluon g and the u, d and s quarks. The charm quark fragments into the $D^{*\pm}$ meson similarly as the gluon and the light quarks with a fragmentation function (FF) known from other processes. The well-known factorization theorem then provides a straightforward procedure for order-by-order perturbative calculations. Although this approach can be used as soon as the factorization scales of the initial and final states are above the starting scale of the parton distribution functions (PDFs) of the (anti)proton and of the FFs of the $D^{*\pm}$ meson, the predictions are reliable only in the region of large transverse momenta $p_T \gg m$, where terms of the order of m^2/p_T^2 can safely be neglected.

Another calculational scheme for heavy-flavor production which could be applied to the process $p + \bar{p} \rightarrow D^{*\pm} + X$ [4–7] is the so-called massive scheme, also called fixed flavor-number (FFN) scheme, in which the number of active quark flavors in the initial state is limited to $n_f = 3$ and the charm quark appears only in the final state. In this case, the charm quark is always treated as a heavy particle and never as a parton. The actual mass parameter m is explicitly taken into account along with the variable p_T as if they were of the same order, irrespective of their actual relative magnitudes. In this scheme, the charm mass acts as a cutoff for the initial- and final-state collinear singularities and sets the scale for the perturbative calculations. However, in NLO, terms proportional to $\alpha_s(\mu_R)\ln(p_T^2/m^2)$, where μ_R is the renormalization scale, arise from collinear emissions of a gluon by the charm quark at large transverse momenta or from almost collinear branchings of gluons into $c\bar{c}$ pairs. These terms are of order unity for large values of p_T and, with the choice $\mu_R \approx p_T$, they spoil the convergence of the perturbation series. The FFN approach with $n_f = 3$ should thus be limited to a rather narrow range of p_T values, reaching up to a few times m.

There are also interpolating schemes, which smoothly interpolate between the FFN scheme at low values of p_T and the ZM-VFN scheme at large values of p_T, with some freedom concerning the detailed implementation. The Aivazis-Collins-Olness-Tung [8] scheme, also known as

general-mass variable-flavor-number (GM-VFN) scheme, is one of them. This scheme was applied to the hadroproduction of heavy flavors in Ref. [9] taking into account the FFN part at NLO and the leading logarithms of the ZM-VFN part.

Another interpolating scheme which has been applied to inclusive $D^{*\pm}$ production in the Tevatron region is the so-called fixed-order next-to-leading-logarithmic (FONLL) scheme, in which the traditional cross section in the FFN scheme and a suitably modified cross section in the ZM-VFN scheme with perturbative FFs are linearly combined [10,11]. The combination is done in such a way, that the ZM-VFN term is weighted with an *ad hoc* coefficient function of the form $p_T^2/(p_T^2 + 25m^2)$ to enforce its suppression in the low-p_T range. In both finite-charm-mass approaches, the FFN and the FONLL, the theoretically calculated FFN cross sections are convoluted with a nonperturbative FF extracted from e^+e^- data. This assumes universality of the FF which is not supported by a factorization theorem as in the ZM-VFN approach.

As has been explained at many places in the literature, mainly in the context of charm production in deep-inelastic ep scattering (for a recent review, see Ref. [12]), the correct approach for $p_T \gg m$ is to absorb the potentially large logarithms into the charm PDF of the (anti)proton and the FF of the $c \to D^{*+}$ transition. Then, large logarithms of the type $\ln(\mu_F^2/m^2)$, defined with the factorization scale μ_F, determine the evolution to higher scales and can be resummed by virtue of the Dokshitzer-Gribov-Lipatov-Altarelli-Parisi (DGLAP) [13] evolution equations. The unsubtracted terms of the form $\ln(p_T^2/\mu_F^2)$ are of order unity for the appropriate choice of μ_F of order p_T. After factorizing the $\ln m^2$ terms, the hard cross section is infrared safe, and $n_f = 4$ is taken in the formula for α_s and the DGLAP evolution equations. The remaining dependence on m, i.e., the terms proportional to m^2/p_T^2, can be kept in the hard cross section to achieve better accuracy in the intermediate region $p_T \gtrsim m$. The factorization of mass-divergent terms can be extended consistently to higher orders in α_s, as has been shown by Collins in the context of heavy-flavor production in high-Q^2 ep collisions [14].

It is well known that the subtraction of just the collinearly (mass) singular terms does not define a unique factorization prescription. Also finite terms must be specified. In the conventional ZM-VFN calculation, the mass m is put to zero from the beginning and the collinearly divergent terms are defined with the help of dimensional regularization. This fixes the finite terms in a specific way, and their form is inherent to the chosen regularization procedure. If one starts with $m \neq 0$ and performs the limit $m \to 0$ afterwards, the finite terms can be different. These terms have to be removed by subtraction together with the $\ln m^2$ terms in such a way that, in the limit $p_T \to \infty$, the known ZM-VFN expressions are recovered. This requirement is actually unavoidable, since almost all existing PDFs and FFs, including those for heavy flavors, are defined in this particular scheme (or sometimes in the deep-inelastic-scattering scheme, which can be derived from the $\overline{\text{MS}}$ scheme). It is clear that a subtraction scheme defined in this way is a correct extension of the conventional ZM-VFN scheme to include charm-quark mass effects in a consistent way. In the following, we shall refer to it as the GM-VFN scheme, since it is conceptually similar to the framework of Ref. [9]. For a fully consistent analysis of heavy-flavor production in $p\bar{p}$ collisions, it will eventually be necessary to use dedicated PDFs and FFs with heavy-quark mass effects included, determined by global fits utilizing massive hard-scattering cross sections. Needless to say that it is, therefore, important to work out massive hard-scattering coefficients in one particular scheme for all relevant processes. Actually, just recently PDFs of the proton with heavy-quark mass effects included have been constructed by members of the CTEQ Collaboration [15] in a scheme very similar to ours as outlined above. If these were used in a calculation of charm production in $p\bar{p}$ collisions, the treatment of the corresponding hard-scattering cross sections would have to be adjusted to these PDFs. However, we think that this would be premature as long as similar constructions of the FF for $c \to D^{*+}$ do not exist.

In a recent work, two of us applied the GM-VFN scheme to the calculation of the cross sections for $\gamma + \gamma \to D^{*\pm} + X$ [16,17] and $\gamma + p \to D^{*\pm} + X$ [18]. In Ref. [17], we considered only the direct and the single-resolved cross sections with $m \neq 0$. In the calculation of the full cross section for $\gamma + \gamma \to D^{*\pm} + X$, needed for the comparison with experimental data, i.e., in the sum of the direct, single-resolved and double-resolved parts, the double-resolved contribution was still treated in the ZM-VFN scheme with $n_f = 4$. It is the purpose of this work to apply the GM-VFN approach to the $p\bar{p}$ cross section. The results of this calculation can then also be applied to the cross sections of double-resolved $\gamma\gamma$ and resolved γp collisions. These cross sections play an important role due to the partonic subprocesses $g + g \to c + \bar{c}$ and $q + \bar{q} \to c + \bar{c}$ with charm quarks in the final state and due to the subprocess $g + q(\bar{q}) \to c + \bar{c} + q(\bar{q})$, where q is one of the light (massless) quarks u, d and s. These contributions and their NLO corrections should be computed with massive charm quarks. Although FFs for various charm mesons have been constructed from e^+e^- data [19], we shall restrict ourselves to inclusive $D^{*\pm}$ production and study the mass-dependent corrections for this special final state only. Results for the inclusive production of other charm mesons will be presented in a future publication.

Starting with $g + g \to c + \bar{c}$, the NLO corrections for this subprocess can be split into an Abelian and two non-Abelian parts. The Abelian part is, up to an overall constant factor, identical to the NLO corrections to $\gamma + \gamma \to c + \bar{c}$.

For this part, the terms in the massive theory surviving in the limit $m \to 0$, which are not present in the ZM-VFN approach, have been identified in our earlier work [16]. Therefore, only the two non-Abelian parts of the NLO corrections to the gluon-gluon fusion cross section have to be investigated in addition to the cross sections for $q + \bar{q} \to c + \bar{c} + g$ and $g + q(\bar{q}) \to c + \bar{c} + q(\bar{q})$.

The NLO corrections with nonzero quark mass m were calculated by several groups [4–7]. In none of these references, complete formulas for the NLO corrections were published. Fortunately, Bojak supplied us with the computer code which was used in Ref. [7]. From this code, we were able to read off the complete NLO squared matrix elements needed for the computation of the mass-dependent cross section. The authors of Ref. [7] compared their results with those of Refs. [5,6] and found complete agreement. Therefore, we use these expressions to derive the limit $m \to 0$ and establish the subtraction terms by comparing to the $\overline{\text{MS}}$-factorized cross section derived in Ref. [20]. The latter is available to us in the form of a FORTRAN program [3,21]. Since, in the work of Ref. [7], the FFN cross section was derived with a method different from the one used in Ref. [16], namely, with the phase-space slicing method for separating the infrared-divergent part from the hard part of the cross section, we also derive the massless limit of the Abelian part for consistency. With this knowledge, we can compute the finite-mass corrections for the full NLO cross section with $\overline{\text{MS}}$ factorization.

The outline of our work is as follows. In Sec. II, we describe the formulas which we use to calculate the cross section for $g + g \to c(\bar{c}) + X$, $q + \bar{q} \to c(\bar{c}) + X$, $g + q \to c(\bar{c}) + X$ and $g + \bar{q} \to c(\bar{c}) + X$ with nonzero charm-quark mass. For these cross sections, we perform the limit $m \to 0$ and compare the results with the ZM-VFN theory of Ref. [20]. The results are collected in Sec. III and three appendices. In Sec. III, we also present numerical results to test the validity of the subtraction terms and show how the various terms in the NLO cross section approach their corresponding massless limits for large values of p_T. After adding the contributions with (anti)charm quarks in the initial state, which are present in the ZM-VFN scheme with $n_f = 4$, as well as the contributions due to the fragmentation of gluons and light (anti)quarks, we compare our results to recent experimental data from the CDF Collaboration [1] in Sec. IV. A summary and conclusions are given in Sec. V.

II. LO AND NLO DIFFERENTIAL CROSS SECTIONS

The differential inclusive cross section for the process $p + \bar{p} \to D^{*\pm} + X$ has many contributions. In this section, we consider those contributions where the charm quark appears only in the final state. We study the charm-quark mass dependence to obtain the massless limit, which is then compared with the ZM-VFN theory, and to establish the influence of the m^2/p_T^2 terms in the GM-VFN theory defined in the same $\overline{\text{MS}}$ factorization scheme as the ZM-VFN theory.

There are only two leading-order (LO) partonic subprocesses, $g + g \to c + \bar{c}$ and $q + \bar{q} \to c + \bar{c}$. The NLO corrections to these two channels comprise the virtual corrections and gluonic bremsstrahlung contributions, $g + g \to c + \bar{c} + g$ and $q + \bar{q} \to c + \bar{c} + g$. In addition, the subprocesses $g + q \to c + \bar{c} + q$ and $g + \bar{q} \to c + \bar{c} + \bar{q}$ appear for the first time at NLO. In the following subsections, we present the LO cross sections in order to fix the notation. Then, we explain how we calculate the NLO corrections to $g + g \to c + \bar{c}$ and $q + \bar{q} \to c + \bar{c}$ and the cross sections for $g + q(\bar{q}) \to c + \bar{c} + q(\bar{q})$.

A. LO cross section

We start with the subprocess

$$g(k_1) + g(k_2) \to c(p_1) + \bar{c}(p_2) + [g(p_3)], \tag{1}$$

where k_1, k_2 and p_i ($i = 1, 2, 3$) denote the four-momenta of the incoming gluons, the outgoing charm and anticharm quarks and a possible gluon in the final state (in square brackets). We have the following invariants:

$$\begin{aligned} &s = (k_1 + k_2)^2, \qquad t_1 = t - m^2 = (k_1 - p_1)^2 - m^2, \\ &u_1 = u - m^2 = (k_2 - p_1)^2 - m^2, \\ &s_2 = (k_1 + k_2 - p_1)^2 - m^2 = s + t_1 + u_1. \end{aligned} \tag{2}$$

Here t_1 and u_1 are determined by the four-momentum of the observed charm quark. As usual, we define the dimensionless variables v and w by

$$v = 1 + \frac{t_1}{s}, \qquad w = -\frac{u_1}{s + t_1}, \tag{3}$$

so that $t_1 = -s(1 - v)$, $u_1 = -svw$ and $s_2 = sv(1 - w)$. For $p_3 = 0$, i.e., at LO, we have $s_2 = 0$ and $w = 1$.

The LO cross section for $g + g \to c + \bar{c}$ is

$$\begin{aligned} \frac{d^2\sigma_{\text{LO}}^{gg}}{dv\,dw} = c(s)\delta(1 - w)&\left(C_F - C_A\frac{t_1u_1}{s^2}\right) \\ &\times\left[\frac{t_1}{u_1} + \frac{u_1}{t_1} + \frac{4m^2s}{t_1u_1}\left(1 - \frac{m^2s}{t_1u_1}\right)\right], \end{aligned} \tag{4}$$

where

$$c(s) = \frac{\pi\alpha_s^2}{(N^2 - 1)s}, \tag{5}$$

and all color factors have been expressed in terms of the Casimir operators $C_F = (N^2 - 1)/(2N)$ and $C_A = N$, where N denotes the number of colors.

The LO cross section for $q + \bar{q} \to c + \bar{c}$ reads

$$\frac{d^2\sigma_{\text{LO}}^{q\bar{q}}}{dv\,dw} = c_q(s)\delta(1 - w)C_F\left(\frac{t_1^2 + u_1^2}{s^2} + \frac{2m^2}{s}\right), \tag{6}$$

where

$$c_q(s) = \frac{\pi\alpha_s^2}{Ns}. \tag{7}$$

B. NLO cross section

Following the notation of Ref. [7], the color decomposition of the NLO squared matrix element for $g + g \to c + \bar{c} + g$ can be written as

$$|M_{gg}|^2 = g^6 E_\epsilon^2 \frac{2}{N^2-1}\Big[C_F^2 D_{\rm QED} + \frac{1}{4}C_A^2 D_{\rm OQ} + \frac{1}{4}C_A(C_A - 2C_F)D_{\rm KQ}\Big], \tag{8}$$

where $g^2 = 4\pi\alpha_s$ is the strong coupling and $E_\epsilon = 1/(1-\epsilon)$ originates from averaging over the gluon spins in $n = 4 - 2\epsilon$ space-time dimensions. The squared matrix element for the virtual corrections to $g + g \to c + \bar{c}$ can be written in a similar fashion; there is, however, an additional contribution from quark loops which comes with a color factor $C_A/4$. The Abelian contribution $D_{\rm QED}$ is identical to the QED part of $\gamma g \to c\bar{c}g$ in Ref. [22]. In addition, we have two non-Abelian parts $D_{\rm OQ}$ and $D_{\rm KQ}$. For isolating the divergences in the soft limit, Bojak and Stratmann [7] used the same method as in Ref. [5]. They slice the $2 \to 3$ contributions into a *soft-gluon* and a *hard-gluon* part by introducing a small auxiliary quantity Δ. In the limit $\Delta \to 0$, the kinematics of the soft-gluon cross section is that of the $2 \to 2$ process, so that the phase-space integrations can be performed analytically. After combination with the virtual cross section, the infrared $1/\epsilon$ and the combined infrared-collinear $1/\epsilon^2$ singularities, all proportional to the n-dimensional LO cross section, cancel. In this way, the *soft plus virtual* cross section becomes finite, except for the remaining collinear $1/\epsilon$ singularities, which cancel against the subtraction terms in the collinear factorization procedure of the gluon PDF of the (anti)proton. The integration over the phase space of the two unobserved partons in the hard part is done analytically as far as possible, using the methods of Refs. [5,6].

The same steps are taken to calculate the NLO corrections to the subprocess $q + \bar{q} \to c + \bar{c}$. The squared matrix element for the real corrections is color-decomposed in the following way:

$$|M_{qq}|^2 = g^6 \frac{1}{2N}\Big(C_F^2 N_{\rm QED} + \frac{1}{2}C_F C_A N_{\rm OK}\Big), \tag{9}$$

where $N_{\rm QED}$ is again the Abelian and $N_{\rm OK}$ the non-Abelian part, which are also obtained from Ref. [7]. A similar decomposition is used for the virtual corrections, which receive an additional contribution from one diagram with a quark loop in the gluon propagator, proportional to the color factor $C_F/2$.

The subprocess

$$g(k_1) + q(k_2) \to c(p_1) + \bar{c}(p_2) + q(p_3), \tag{10}$$

which occurs only in NLO, has two pieces in color space. The squared matrix element is split up according to

$$|M_{gq}|^2 = g^6 E_\epsilon \frac{1}{4N}\Big(C_F J_{\rm QED} + \frac{1}{2}C_A J_{\rm OK}\Big). \tag{11}$$

The Abelian part $J_{\rm QED}$ is, up to a factor, equal to the corresponding squared matrix element for the subprocess $\gamma + q \to c + \bar{c} + q$. The squared matrix element for the crossed subprocess $g + \bar{q} \to c + \bar{c} + \bar{q}$, i.e., Eq. (10) with the quark replaced by an antiquark, has the same structure as in Eq. (11), but with slightly different coefficients.

III. ZERO-MASS LIMIT OF THE MASSIVE CROSS SECTIONS

In this section, we collect our results for the cross sections in the limit $m \to 0$. We consider the following contributions: (i) the NLO corrections to $g + g \to c + \bar{c}$, (ii) the NLO corrections to $q + \bar{q} \to c + \bar{c}$ and (iii) the process $g + q \to c + \bar{c} + q$ and the corresponding channel with $q \to \bar{q}$, where q denotes any of the light (massless) quarks u, d and s. The result for the limit $m \to 0$ will in general be different from the cross section obtained in the ZM-VFN approach, where the mass of the charm quark is neglected from the beginning. In the genuine ZM-VFN calculation, originally performed by Aversa *et al.* [20], the collinear singularities connected with the charm quark appear as $1/\epsilon$ poles in dimensional regularization. In the FFN theory, they appear as terms proportional to $\ln(m^2/s)$, instead. So, in this theory, the collinear singularities are regularized with a finite charm mass. Because of this different procedure for regularizing the collinearly divergent contributions, different finite terms appear. The occurrence of different finite terms in these two regularization schemes is due to the fact that the two limits, $m \to 0$ and $\epsilon \to 0$, are not interchangeable. If one wants to implement the factorization of these collinearly singular terms in the $\overline{\rm MS}$ scheme, as is done in the ZM-VFN scheme from the start, the different finite terms, which turn up in the limit $m \to 0$, must be subtracted. Such finite terms have already been found for the case of the NLO corrections to $\gamma + \gamma \to c + \bar{c}$ [16] and $\gamma + g \to c + \bar{c}$ and for the cross section of $\gamma + q \to c + \bar{c} + q$ [17].

As in Refs. [16,17], we decompose the NLO contributions to the cross section in the limit $m \to 0$ as follows:

$$\lim_{m\to 0}\frac{d^2\sigma_{\rm NLO}}{dvdw} = \left(c_1 + \tilde{c}_1 \ln\frac{m^2}{s}\right)\delta(1-w) + \left(c_2 + \tilde{c}_2 \ln\frac{m^2}{s}\right)\left(\frac{1}{1-w}\right)_+ + c_3\left[\frac{\ln(1-w)}{1-w}\right]_+ + c_5 \ln v + c_6 \ln(1-vw)$$
$$+ c_7 \ln(1-v+vw) + c_8 \ln(1-v) + c_9 \ln w + c_{10}\ln(1-w) + c_{11} + \tilde{c}_{11}\ln\frac{m^2}{s}$$
$$+ c_{12}\frac{\ln(1-v+vw)}{1-w} + c_{13}\frac{\ln w}{1-w} + c_{14}\frac{\ln(\frac{1-v}{1-vw})}{1-w}. \quad (12)$$

The coefficients c_i are mass-independent; the dependence on the heavy-quark mass enters only through the logarithms $\ln(m^2/s)$ and the choice $\mu_R = \mu_F = m$.

In the following subsections, we shall present the complete expressions for the coefficients c_i. The massless limit of the cross sections from Ref. [7] will be compared with the results of Ref. [20] obtained in the ZM-VFN theory.

A. Massless limit of NLO corrections to $g + g \to c + \bar{c}$

Before we write down the coefficients c_i, we give the LO cross section for $g + g \to c + \bar{c}$ with $m = 0$. It has the simple form

$$\lim_{m\to 0}\frac{d^2\sigma^{gg}_{\rm LO}}{dvdw} = c(s)\delta(1-w)\tau(v)[C_F - C_A v(1-v)], \quad (13)$$

with

$$\tau(v) = \frac{v}{1-v} + \frac{1-v}{v}. \quad (14)$$

The results for the various coefficients c_i are written in the form

$$c_i = \hat{c}_i + \Delta c_i, \quad (15)$$

where $\hat{c}_i$ are the results of Ref. [20] in the ZM-VFN scheme and Δc_i are the subtraction terms needed to convert the cross section of Ref. [7] to the GM-VFN scheme. The coefficients are decomposed into one Abelian part, two non-Abelian parts and a quark-loop contribution (which only occurs for c_1) in the following way:

$$c_i = C(s)\Big[C_F^2 c_i^{\rm qed} + \frac{1}{4}C_A^2 c_i^{\rm oq} + \frac{1}{4}C_A(C_A - 2C_F)c_i^{\rm kq} + \delta_{i1}\frac{C_A}{4}c_1^{\rm ql}\Big], \quad (16)$$

with

$$C(s) = \frac{\alpha_s^3}{2(N^2-1)s} = \frac{\alpha_s}{2\pi}c(s). \quad (17)$$

The expressions for the c_i are lengthy and, therefore, delegated to Appendix A.

The coefficients $\hat{c}_i$, which agree with results obtained from Ref. [20], refer to the version where every incoming-gluon spin is averaged with the factor $1/[2(1-\epsilon)]$ and where the factorization of singularities due to collinear quarks and gluons is performed in the customary $\overline{\rm MS}$ subtraction scheme. Furthermore, deviating from Ref. [20], in the expressions for $\hat{c}_i$ in Appendix A, the renormalization scale μ_R and the initial- and final-state factorization scales μ_F and μ_F' are identified with m, i.e., $\mu_R = \mu_F = \mu_F' = m$. The nonvanishing subtraction terms in the massless limit of the FFN theory of Ref. [7] are found in Appendix A. They are Δc_1, Δc_2, Δc_3, Δc_5, Δc_{10} and Δc_{11}. For all three contributions $c_i^{\rm qed}$, $c_i^{\rm oq}$ and $c_i^{\rm kq}$, we have the relation

$$\Delta c_5 = \Delta c_{10} = 2\Delta c_{11}. \quad (18)$$

Denoting the ZM-NLO result of Ref. [20] by $d^2\sigma_{\rm ZM}/dvdw$, we can thus write

$$\lim_{m\to 0}\frac{d^2\sigma_{\rm NLO}}{dvdw} = \frac{d^2\sigma_{\rm ZM}}{dvdw}(\mu_R = \mu_F = \mu_F' = m) + \frac{d^2\sigma_{\rm sub}}{dvdw}, \quad (19)$$

where

$$\frac{d^2\sigma_{\rm sub}}{dvdw} = \Delta c_1\delta(1-w) + \Delta c_2\left(\frac{1}{1-w}\right)_+ + \Delta c_3\left[\frac{\ln(1-w)}{1-w}\right]_+ + \Delta c_5\left[\ln v + \ln(1-w) + \frac{1}{2}\right]. \quad (20)$$

For the first three subtraction terms proportional to Δc_1, Δc_2 and Δc_3, one obtains simple expressions, if the three contributions in Eq. (16) proportional to the color factors C_F^2, C_A^2 and $C_A(C_A - 2C_F)$ are added. From the results in Appendix A, we obtain

$$\Delta c_1 = (1 - \ln v - \ln^2 v)\times 2C(s)C_F\tau(v)[C_F - C_A v(1-v)], \quad (21)$$

$$\Delta c_2 = -(2\ln v + 1)\times 2C(s)C_F\tau(v)[C_F - C_A v(1-v)], \quad (22)$$

$$\Delta c_3 = -2\times 2C(s)C_F\tau(v)[C_F - C_A v(1-v)], \quad (23)$$

and

$$\Delta c_5 = C(s)C_F(C_F\Delta c_5^{\rm qed} + \tfrac{1}{2}C_A\Delta c_5^{\rm oq}). \quad (24)$$

In the last equation, we have used $\Delta c_5^{\rm kq} = -\Delta c_5^{\rm oq}$; the explicit expressions for these coefficients are given in Appendices A 2 and A 3. Note that the last factors in Eqs. (21)–(23) are proportional to the LO cross section. Finally, we have to subtract the quark-loop contribution,

which is absent in the ZM-VFN scheme, via [23]

$$\Delta c_1 \to \Delta c_1 + C(s)\frac{C_A}{4}\Delta c_1^{\rm ql} = \Delta c_1 - C(s)C_A\frac{1}{9}v(1-v). \tag{25}$$

The FFN theory for $g + g \to c + X$ in the limit $m \to 0$ approaches the ZM-VFN theory with scales $\mu_R = \mu_F = \mu_F' = m$ if the finite terms Δc_1, Δc_2, Δc_3 and $\Delta c_5 = \Delta c_{10} = 2\Delta c_{11}$ as given in Eqs. (21)–(24) are subtracted. As already mentioned above, the necessity for such a subtraction is to be expected, since the regularization of collinear singularities with a mass parameter m does not give the same result as the one with dimensional regularization and $m = 0$ from the start.

In Ref. [16], it was shown that the finite subtraction terms for the subprocess $\gamma + \gamma \to c + X$ can be obtained by a convolution of the LO cross section with a perturbative partonic FF $d_c^c(x, \mu)$ for the transition from a massless to a massive charm quark of the following form [24]:

$$d_c^c(x,\mu) = C_F\frac{\alpha_s}{2\pi}\left\{\frac{1+x^2}{1-x}\left[\ln\frac{\mu^2}{m^2} - 2\ln(1-x) - 1\right]\right\}_+. \tag{26}$$

Therefore, all Abelian terms proportional to C_F^2 in Eqs. (21)–(24) can also be generated in this way. Our explicit calculations show that also all terms proportional to $C_F C_A$ in the equations above can be obtained as final-state interaction contributions with $d_c^c(x, \mu)$ in Eq. (26) [without the term proportional to $\ln(\mu^2/m^2)$, of course].

It is important to understand that the terms containing logarithms $\ln(m^2/s)$, i.e., the coefficients $\tilde{c}_1$, $\tilde{c}_2$ and $\tilde{c}_{11}$, have two different origins. On the one hand, these terms are due to on-shell internal charm-quark lines in the Feynman diagrams which become singular for $m \to 0$ [see Figs. 1(a) and 1(c)]. A part of these terms [see Fig. 1(a)] is contained in the perturbative FFs $d_c^c(x, \mu)$. Also internal gluon and light-quark lines give rise to singular contributions for $m \to 0$ [see Fig. 1(b)], which have to be factorized into corresponding perturbative FFs describing the transition from a gluon or a light quark to the heavy charm quark. In the ZM-VFN calculation, these contributions have been factorized as final-state singularities and are recovered by setting $\mu_F' = m$. Another part of these singular terms can be assigned to the initial state [see Fig. 1(c)], and is found in the ZM-VFN calculation if one sets $\mu_F = m$. On the other hand, in both the FFN and ZM-VFN calculations, there are singularities due to internal gluon lines which are, in both approaches, factorized as initial-state singularities [see Fig. 1(d)]. Finally, there are logarithms due to the renormalization of α_s. In Appendix A, these terms are written down for the choice $\mu_R = \mu_F = \mu_F' = m$.

For our application, choosing the scales equal to the heavy-quark mass is not appropriate. For the case of large p_T values, a common choice is $\mu_R = \mu_F = \mu_F' = \xi m_T$,

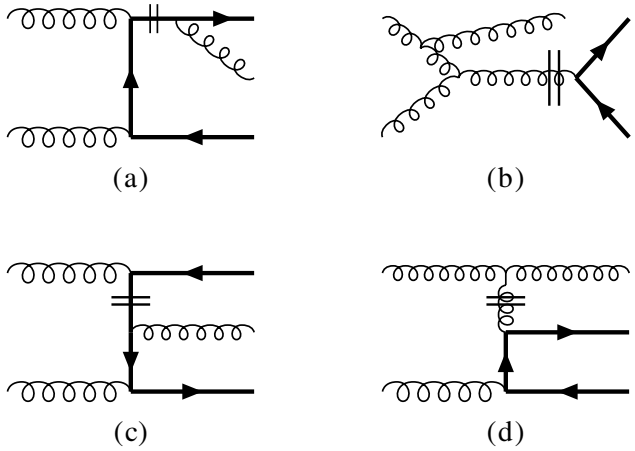

FIG. 1. Sample Feynman diagrams showing the origin of mass singularities due to internal lines becoming on-shell (marked by a double line). Parts (a) and (b) correspond to singularities for $m \to 0$ which are factorized into the final-state FF; parts (c) and (d) are examples for singular configurations which are factorized into the initial-state PDFs.

where $m_T = \sqrt{m^2 + p_T^2}$ is the transverse mass of the $D^{*\pm}$ meson and $\xi = \mathcal{O}(1)$. Therefore, we have to rescale all terms proportional to $\ln m^2$. In the following, we shall give the necessary terms for the conversion to arbitrary scales.

First, we present the contributions related to renormalization and initial-state factorization of singularities due to internal on-shell gluon lines. These terms are present in the FFN calculation and can, therefore, be obtained from Ref. [7] in the limit $m \to 0$. The rescaling is obtained by adding the following terms to the cross section in Eq. (12):

$$\left(\frac{d^2\sigma}{dv\,dw}\right)_{\rm rescal} = \left(\hat{d}_1\ln\frac{\mu_R^2}{m^2} + \tilde{d}_1\ln\frac{\mu_F^2}{m^2} + \tilde{\tilde{d}}_1\ln\frac{\mu_F'^2}{m^2}\right) \times \delta(1-w) + \left(\tilde{d}_2\ln\frac{\mu_F^2}{m^2} + \tilde{\tilde{d}}_2\ln\frac{\mu_F'^2}{m^2}\right) \times \left(\frac{1}{1-w}\right)_+ + \tilde{d}_{11}\ln\frac{\mu_F^2}{m^2} + \tilde{\tilde{d}}_{11}\ln\frac{\mu_F'^2}{m^2}. \tag{27}$$

The nonzero coefficients read

$$\hat{d}_1 = C(s)\tau(v)2\beta_0^{(n_f-1)}[C_F - C_A v(1-v)], \tag{28}$$

$$\tilde{d}_1 = C(s)\tau(v)[C_F - C_A v(1-v)]\{2C_A[\ln(1-v) - \ln(v)] - 2\beta_0^{(n_f-1)}\}, \tag{29}$$

$$\tilde{d}_2 = -C(s)\tau(v)4C_A[C_F - C_A v(1-v)], \tag{30}$$

$$\tilde{d}_{11} = C(s)\left[\frac{C_A^2}{4}\tilde{d}_{11}^{\rm oq} + \frac{C_A(C_A - 2C_F)}{4}\tilde{d}_{11}^{\rm kq}\right], \tag{31}$$

with $\beta_0^{(n_f)} = 11N/6 - n_f/3$ and

$$\tilde{d}_{11}^{\,\mathrm{oq}} = \frac{4(-1+5v-12v^2+20v^3-12v^4+4v^5)}{v_1^2 v} - \frac{4(1-4v+8v^2-8v^3+4v^4)}{v_1 v w^2} - \frac{4(3-9v+14v^2-11v^3+4v^4)}{v_1^2 w} - \frac{4(-1+5v-12v^2+28v^3-24v^4+12v^5)w}{v_1^2 v} + \frac{16v^3(1+v)w^2}{v_1^2} - \frac{16v^4 w^3}{v_1^2} + \frac{4v_1 v}{X^3} + \frac{4v(-4+3v)}{X^2} + \frac{4v(10-13v+5v^2)}{v_1 X}, \tag{32}$$

$$\tilde{d}_{11}^{\,\mathrm{kq}} = \frac{-4(-1+3v-4v^2+4v^3)}{v_1^2 v} + \frac{4(1-2v+2v^2)}{v_1 v w^2} + \frac{4(1-v+v^3)}{v_1^2 w} + \frac{4(-1+3v-4v^2+4v^3)w}{v_1^2 v} - \frac{4v_1 v}{X^3} + \frac{4v_2 v}{X^2} - \frac{4v(4-3v+v^2)}{v_1 X}, \tag{33}$$

where we have used the abbreviations $X = 1 - vw$ and $v_i = i - v$. We repeat that the expressions above are given in the limit $m \to 0$ and will be used in our ZM-VFN calculation with rescaling. In the GM-VFN calculation, we shall use instead the corresponding terms as given in Ref. [7] including their full mass dependence.

Finally, the remaining logarithms emerging in the limit $m \to 0$ due to internal charm-quark lines becoming massless are again found by comparing the massless limit of the FFN cross section with the ZM-VFN cross section. These terms are associated with a rescaling of the subtraction terms in Eq. (20), and, therefore, we write them in the following form:

$$\left(\frac{d^2\sigma}{dv\,dw}\right)_{\Delta\mathrm{rescal}} = \left(\Delta\hat{d}_1 \ln\frac{\mu_R^2}{m^2} + \Delta\tilde{d}_1 \ln\frac{\mu_F^2}{m^2} + \Delta\tilde{\tilde{d}}_1 \ln\frac{\mu_F'^2}{m^2}\right) \times \delta(1-w) + \left(\Delta\tilde{d}_2 \ln\frac{\mu_F^2}{m^2} + \Delta\tilde{\tilde{d}}_2 \ln\frac{\mu_F'^2}{m^2}\right) \times \left(\frac{1}{1-w}\right)_+ + \Delta\tilde{d}_{11} \ln\frac{\mu_F^2}{m^2} + \Delta\tilde{\tilde{d}}_{11} \ln\frac{\mu_F'^2}{m^2}. \tag{34}$$

These terms must be added to Eq. (20), i.e., *subtracted* from Eq. (12), to rescale to the appropriate renormalization and factorization scales if one wants to use the FF for the transition $c \to D^{*+}$ and the charm PDF of the (anti)proton. Since, at present, we have at our disposal only PDFs and FFs, which are based on a ZM-VFN calculation, we shall take the corresponding coefficients for $m = 0$ as well. Note that this does not entail any loss of accuracy, as has been discussed in Ref. [25] in the context of deep-inelastic scattering. Moreover, this fact is of great practical importance, since the known coefficients of the ZM-VFN scheme, e.g., those of Ref. [20], can simply be used, whereas their massive counterparts are unknown and can only be obtained through a dedicated calculation. The nonzero coefficients are given by

$$\Delta\hat{d}_1 = \tfrac{2}{3} C(s)\tau(v)[C_F - C_A v(1-v)], \tag{35}$$

$$\Delta\tilde{d}_1 = -\tfrac{2}{3} C(s)\tau(v)[C_F - C_A v(1-v)], \tag{36}$$

$$\Delta\tilde{\tilde{d}}_1 = C(s)\tau(v)C_F(2\ln v + \tfrac{3}{2})[C_F - C_A v(1-v)], \tag{37}$$

$$\Delta\tilde{\tilde{d}}_2 = 2C(s)\tau(v)C_F[C_F - C_A v(1-v)], \tag{38}$$

$$\Delta\tilde{\tilde{d}}_{11} = C(s)\left[C_F^2 \Delta\tilde{\tilde{d}}_{11}^{\mathrm{qed}} + \frac{C_A^2}{4}\Delta\tilde{\tilde{d}}_{11}^{\mathrm{oq}} + \frac{C_A(C_A - 2C_F)}{4}\Delta\tilde{\tilde{d}}_{11}^{\mathrm{kq}}\right], \tag{39}$$

$$\Delta\tilde{d}_{11} = C(s)\left[C_F^2 \Delta\tilde{d}_{11}^{\mathrm{qed}} + \frac{C_A^2}{4}\Delta\tilde{d}_{11}^{\mathrm{oq}} + \frac{C_A(C_A - 2C_F)}{4}\Delta\tilde{d}_{11}^{\mathrm{kq}}\right], \tag{40}$$

with

$$\Delta\tilde{d}_{11}^{\,\mathrm{qed}} = -\frac{v}{v_1} + \frac{2-2v+v^2}{vw} - \frac{v^2 w}{v_1} - \frac{2v}{Y}, \tag{41}$$

$$\Delta\tilde{d}_{11}^{\,\mathrm{oq}} = 2v(1-24v) + \frac{8v_1(1-2v+2v^2)}{vw^2} + \frac{16(1-3v+2v^2)}{w} + \frac{8v^2(7-14v+8v^2)w}{v_1^2} - \frac{16v^3(-1+2v)w^2}{v_1^2} + \frac{16v^4 w^3}{v_1^2} + \frac{4vv_1^2}{Y^3} - \frac{4v(6-11v+5v^2)}{Y^2} + \frac{2v(25-18v+4v^2)}{Y}, \tag{42}$$

$$\Delta\tilde{d}_{11}^{\,\mathrm{kq}} = -2v + \frac{4vv_1^2}{Y^3} - \frac{4v^2 v_1}{Y^2} + \frac{2v(3-6v+4v^2)}{Y}, \tag{43}$$

$$\Delta\tilde{d}_{11}^{\rm qed} = -\frac{2-2v+3v^2-4v^3}{v_1 v} + \frac{1+v^2}{vw} - \frac{(-2+2v-2v^2+3v^3)w}{v_1 v} + \frac{2vv_1}{X^3} - \frac{2v}{X^2} - \frac{v(-3+4v-2v^2)}{v_1 X}, \tag{44}$$

$$\Delta\tilde{d}_{11}^{\rm oq} = -\frac{2(2-v+3v^2)}{v_1^2} + \frac{4(1-2v+2v^2)}{v_1 v w^2} - \frac{2(-3+10v-13v^2+4v^3)}{v_1^2 w} + \frac{4(1+v^2)w}{v_1^2} + \frac{4v_1 v}{X^2} - \frac{4v(-1+2v)}{X}, \tag{45}$$

$$\Delta\tilde{d}_{11}^{\rm kq} = -\Delta\tilde{d}_{11}^{\rm oq}, \tag{46}$$

where $Y = 1 - v + vw$.

Comparing with the results for $\gamma + \gamma \to c + X$ [16], we see that the Abelian parts of Eqs. (37) and (38) agree with $-\tilde{\tilde{c}}_1$ and $-\tilde{\tilde{c}}_2$ in Ref. [16] [if the $C(s)$ factors are set to unity]. Furthermore, $\Delta\tilde{\tilde{d}}_{11}^{\rm qed}$ agrees with $-\tilde{\tilde{c}}_{11}$ and $\Delta\tilde{d}_{11}^{\rm qed}$ with $-\tilde{c}_{11}$ in Ref. [16], as one would expect. The minus sign is due to the different convention for the logarithms in Eq. (42) in Ref. [16] as compared to Eq. (34). We note that $\Delta\tilde{\tilde{d}}_{11}^{\rm qed} = -\Delta c_{11}^{\rm qed}$ and $\Delta\tilde{\tilde{d}}_{11}^{\rm kq} = -\Delta c_{11}^{\rm kq}$ (see Appendices A 1 and A 3, respectively). Finally, we emphasize again that the rescaling of the $\ln m^2$ terms to arbitrary scales μ_R, μ_F and μ_F' is achieved by adding Eq. (27) to and subtracting Eq. (34) from the cross section in Eq. (12), where all coefficients of Eqs. (28)–(40) have to be taken into account. Note also that $\Delta\hat{d}_1$ and $\Delta\tilde{d}_1$ cancel if $\mu_R = \mu_F$.

B. Massless limit of NLO corrections to $q + \bar{q} \to c + \bar{c}$

In this section, we give the results for the massless limit of the hard-scattering cross sections for the NLO corrections to the subprocess $q + \bar{q} \to c + \bar{c}$, where q is any of the light quarks assumed to be massless. The LO cross section of this process for $m = 0$ is

$$\lim_{m\to 0} \frac{d^2\sigma_{\rm LO}^{q\bar{q}}}{dv\,dw} = c_q(s) C_F \tau_q(v) \delta(1-w), \tag{47}$$

where

$$\tau_q(v) = (1-v)^2 + v^2. \tag{48}$$

The NLO cross section is again decomposed as indicated in Eq. (12) with coefficients c_i which receive contributions from two color factors and from virtual-quark loops (which only appear for c_1 and $\tilde{c}_1$). Specifically, we have

$$c_i = C_q(s)\frac{C_F}{2}(C_F c_i^{\rm cf} + C_A c_i^{\rm ca} + \delta_{i1} c_1^{\rm ql}), \tag{49}$$

where

$$C_q(s) = \frac{\alpha_s^3}{2Ns} = \frac{\alpha_s}{2\pi} c_q(s). \tag{50}$$

The expressions for $c_i^{\rm cf}$, $c_i^{\rm ca}$ and $c_1^{\rm ql}$ may be found in Appendix B. According to these results, finite subtraction terms in the massless limit of Ref. [7] are present in c_1, c_2, c_3, c_5, c_{10} and c_{11}, and we have $\Delta c_5 = \Delta c_{10} = 2\Delta c_{11}$ as in the preceding subsection. The first three Δc_i terms have the following simple form:

$$\Delta c_1 = (1 - \ln v - \ln^2 v) \times 2 C_q(s)\tau_q(v) C_F^2, \tag{51}$$

$$\Delta c_2 = -(1 + 2\ln v) \times 2 C_q(s)\tau_q(v) C_F^2, \tag{52}$$

$$\Delta c_3 = -2 \times 2 C_q(s)\tau_q(v) C_F^2, \tag{53}$$

and

$$\Delta c_5 = 2 C_q(s) C_F^2 \left(v - \frac{2vv_1^2}{Y^3} + \frac{2v^2 v_1}{Y^2} - \frac{3v - 6v^2 + 4v^3}{Y} \right). \tag{54}$$

The complete subtraction contribution for the $q\bar{q}$ cross section has the form of Eq. (20) with the Δc_i terms given in Eqs. (51)–(54) and Appendix B. Again, the subtraction terms agree with the convolution of the perturbative FF of Eq. (26) with the LO $q\bar{q}$ cross section. We remark that the Δc_i terms only appear in the QED part.

As in the gg channel, the results in Appendix B are given for the choice $\mu_R = \mu_F = \mu_F' = m$. For our application, we need the cross section for arbitrary scales. To make the transition, we use Eq. (27), where the nonzero contributions to the coefficients $\hat{d}_i$, $\tilde{d}_i$ and $\tilde{\tilde{d}}_i$ have the following form:

$$\hat{d}_1 = C_q(s)\frac{C_F}{2}\tau_q(v) 4\beta_0^{(n_f-1)}, \tag{55}$$

$$\tilde{d}_1 = -C_q(s)\tau_q(v) C_{\rm F}^2 [3 + 2\ln v - 2\ln(1-v)], \tag{56}$$

$$\tilde{d}_2 = -4 C_q(s)\tau_q(v) C_F^2, \tag{57}$$

$$\tilde{d}_{11} = C_q(s) C_F^2 \left[\frac{1 - 8v + 12v^2 - 6v^3}{v_1} - \frac{1 - 2v + 2v^2}{w} + \frac{2v_2 v^2 w}{v_1} - \frac{2v^3 w^2}{v_1} + \frac{v}{X} \right]. \tag{58}$$

Of course, for the calculation of the GM-VFN cross section, the corresponding mass-dependent contributions are used as given in Ref. [7]. These terms rescale all the $\ln m^2$ contributions due to the renormalization and the factorization of internal light-quark lines. Therefore, the shift from renormalization due to internal quark loops is proportional to $\beta_0^{(n_f-1)}$.

To eliminate all $\ln m^2$ terms, we must also take into account the contribution from charm-quark loops and the one from internal charm-quark lines that is factorized into

the FF. These terms are taken into account by using Eq. (34), and the corresponding coefficients are given by

$$\Delta\hat{d}_1 = C_q(s)\tau_q(v)\tfrac{2}{3}C_F, \tag{59}$$

$$\Delta\tilde{\hat{d}}_1 = C_q(s)\tau_q(v)\frac{C_F^2}{2}(3+4\ln v), \tag{60}$$

$$\Delta\tilde{\hat{d}}_2 = C_q(s)\tau_q(v)2C_F^2, \tag{61}$$

$$\Delta\tilde{\hat{d}}_{11} = C_q(s)\left(\frac{C_F^2}{2}\Delta\tilde{\hat{d}}_{11}^{\rm cf} + \frac{C_F C_A}{2}\Delta\tilde{\hat{d}}_{11}^{\rm ca}\right), \tag{62}$$

where

$$\Delta\tilde{\hat{d}}_{11}^{\rm cf} = \frac{2v(2-3v+2v^2)}{v_1} + \frac{2(1-2v+2v^2)}{w} - \frac{4v^3 w}{v_1} + \frac{4v^3w^2}{v_1} + \frac{4vv_1^2}{Y^3} - \frac{4v^2v_1}{Y^2} + \frac{2v(1-6v+4v^2)}{Y}, \tag{63}$$

$$\Delta\tilde{\hat{d}}_{11}^{\rm ca} = 4v_2 v - 4v^2 w - \frac{4vv_1^2}{Y^3} + \frac{4v(3-5v+2v^2)}{Y^2} - \frac{2v(9-12v+4v^2)}{Y}. \tag{64}$$

In the general case, the contributions written down in Eqs. (55)–(58) have to be added and the contributions in Eqs. (59)–(62) have to be subtracted.

C. Massless limit of $g + q \to c + \bar{c} + q$ and $g + \bar{q} \to c + \bar{c} + \bar{q}$

The processes $g + q \to c + \bar{c} + q$ and $g + \bar{q} \to c + \bar{c} + \bar{q}$ appear for the first time at NLO. In the massless limit, the corresponding cross sections are decomposed as explained in Eq. (12). Since there is no LO part, one has $c_1 = c_2 = c_3 = 0$. The remaining coefficients are decomposed with respect to the color factors C_F and C_A as

$$c_i = C_q(s)(C_F c_i^{\rm cf} + C_A c_i^{\rm ca}). \tag{65}$$

The resulting coefficients $c_i^{\rm cf}$ and $c_i^{\rm ca}$ are given in Appendix C for the case that the observed transverse momentum is due to the charm quark. If the anticharm quark is observed with a given value of p_T, the coefficients are different. The differences $c_i^{\bar{c}-c} = c_i(\bar{c}_{\rm observed}) - c_i(c_{\rm observed})$ are listed in Appendix D. Charge conjugation invariance relates the cross sections for quarks and antiquarks in the initial state as $d\sigma/dp_T(g + q \to c_{\rm observed} + \bar{c} + q) = d\sigma/dp_T(g + \bar{q} \to \bar{c}_{\rm observed} + c + \bar{q})$.

We find that, for all gq and $g\bar{q}$ channels, there are no extra finite subtraction terms, i.e., we have $\Delta c_i = 0$ in all cases. Comparing the coefficients $c_i^{\rm cf}$ and $c_i^{{\rm cf},\bar{c}-c}$ with the results for $\gamma + q \to c + \bar{c} + q$ given in Ref. [17], we find agreement, except for Δc_{11}, which was found to be nonzero for $\gamma + q \to c + \bar{c} + q$. The subtraction terms in Ref. [17] were obtained by matching the FFN result of Ref. [26] with the ZM-VFN result of Ref. [27]. In order to clarify this mismatch, we compare the formula for $\gamma + q \to c + \bar{c} + q$ of Ref. [27] with the one from Ref. [28], which we extracted from the FORTRAN program used in that paper, to find that the two disagree. On the other hand, the result in Ref. [28] agrees with the Abelian part of the result for $g + q \to c + \bar{c} + q$ in Ref. [20]. Relying on Ref. [28], we then conclude that we also have $\Delta c_{11} = 0$ for $\gamma + q \to c + \bar{c} + q$ in Ref. [17].

As in the previous cases, the formulas written down in Appendix C are for the scale choice $\mu_R = \mu_F = \mu_R' = m$. The transition to arbitrary scales μ_R, μ_F and μ_F' is obtained, as above, using Eq. (27) with the appropriate coefficients. In the present case, $\tilde{d}_1$ and $\tilde{d}_2$ do not contribute, only $\tilde{d}_{11}$ is nonzero. If we factor out $C_q(s)$, C_F and C_A as in Eq. (65), we obtain the coefficients $\tilde{d}_i^{\rm cf}$ and $\tilde{d}_i^{\rm ca}$, which correspond to the initial-state factorization of singularities due to internal gluons, in the following form:

$$\tilde{d}_{11}^{\rm cf} = \frac{1-4v+9v^2-6v^3+2v^4}{v_1^2} + \frac{-1+2v-4v^2+3v^3-v^4}{v_1^2 w} - \frac{(1-4v+9v^2-6v^3+2v^4)w}{v_1^2} - \frac{v}{2X^2} + \frac{v(3-v)}{2v_1 X}, \tag{66}$$

$$\tilde{d}_{11}^{\rm ca} = \frac{v^2}{v_1^2} - \frac{v^2(2+v^2)w}{v_1^2} + \frac{2v^3(1+v)w^2}{v_1^2} - \frac{2v^4w^3}{v_1^2} + \frac{v}{2X}. \tag{67}$$

In addition, we need the rescaling terms associated with initial-state singularities of internal charm-quark lines and of final-state singularities of gluon lines splitting into $c\bar{c}$ pairs. These contributions vanish for the choice $\mu_F = \mu_F' = m$, which is used in Appendix C. To convert the cross sections to arbitrary factorization scales μ_F and μ_F', we have to take into account the additional rescaling terms denoted as $\Delta\tilde{d}_i$ and $\Delta\tilde{\hat{d}}_i$,

$$\Delta\tilde{d}_{11}^{\rm cf} = \frac{1+v^2}{2v_1^2 w}(1-2w+2w^2), \tag{68}$$

$$\Delta\tilde{\hat{d}}_{11}^{\rm cf} = -2v^2(1-w) + \frac{1-2v+2v^2}{2w} - \frac{v_1 v}{2Y^2} + \frac{v(3-2v)}{2Y}, \tag{69}$$

$$\Delta\tilde{\hat{d}}_{11}^{\rm ca} = -v^2 + \frac{v^2(2-4v+3v^2)w}{v_1^2} - \frac{2v^3(-1+2v)w^2}{v_1^2} + \frac{2v^4w^3}{v_1^2} + \frac{v}{2Y}. \tag{70}$$

D. Numerical test of subtraction terms and study of mass-dependent corrections

The calculation of the subtraction terms, in particular, those in Secs. III A and III B, was rather involved. Special care had to be exercised in order to recover all the terms proportional to $\delta(1-w)$, $1/(1-w)_+$, $[\ln(1-w)/(1-w)]_+$ and the remaining terms in the decomposition of Eq. (12). In particular, the delta-function terms were difficult to calculate, since they received contributions from several places, the virtual corrections and both the soft and hard parts of the real corrections. Some of these contributions contained a dependence on the slicing parameter. The cancellation of these contributions in the final results provided a partial check of our analytical calculations, in particular, for the coefficients of the two plus-distributions.

In order to check that the Δc_i terms presented in Secs. III A and III B are correct, and also to see how the various contributions to $d^2\sigma^{ab}/dvdw$ (where ab stands for the channels gg, $q\bar{q}$, gq and $g\bar{q}$) written down in Sec. II B behave as functions of the transverse momentum p_T of the $D^{*\pm}$ meson, we calculate the NLO corrections in four different ways:

(1) Using the results of Ref. [7], we calculate the cross sections for the channels gg $(g+g \to c+X)$, $q\bar{q}$ $(q+\bar{q} \to c+X)$ and gq $[g+q(\bar{q}) \to c+X]$ in the FFN scheme. The corresponding results will be labeled by σ_m (massive calculation).

(2) We calculate the same cross sections in the limit $m \to 0$, using Eq. (12) with the corresponding coefficients as given in Sec. III and the appendices. Notice that m is kept at its physical value whenever it appears logarithmically in Eq. (12). The results will be denoted σ_0 (massless limit of the massive calculation).

For both the massive calculation and its massless limit, we shall then consider the effect of the subtraction terms described by the coefficients Δc_i:

(3) The subtracted massive calculation, denoted by σ_m^Δ, is obtained by subtracting Eq. (20) with the corresponding coefficients written down in the appendices from σ_m. This corresponds to the GM-VFN scheme.

(4) The subtracted massless cross sections are calculated by subtracting Eq. (20) from σ_0 and will be denoted by σ_0^Δ. This prescription is identical to the ZM-VFN scheme.

In all cases, we start from a calculation using $\mu_R = \mu_F = \mu_F' = m$ and take into account the rescaling to other renormalization and factorization scales in two steps:

(i) We rescale to $\mu_R = \mu_F = \mu_F' = 2m_T$. This scale choice is to prevent the value of μ_F' from falling below the starting scale $2m$ for the μ_F' evolution of the FF for low values of p_T. Firstly, we add the terms due to renormalization and initial-state factorization of singularities related to internal gluon lines, according to Eq. (27).

(ii) Finally, we subtract the remaining rescaling terms of Eq. (34) related to internal charm-quark lines which become singular in the limit $m \to 0$.

In the following, we always normalize the cross sections to the LO ZM-VFN cross sections calculated from Eqs. (4) and (6), i.e., we consider the cross section ratios R_{ab} given by

$$R_{ab} = \frac{d\sigma^{ab}/dp_T}{d\sigma^{ab}_{\rm LO}/dp_T(m=0)}. \tag{71}$$

For the gq and $g\bar{q}$ channels, we normalize to the LO ZM-VFN gg cross section, since, for the gq channel, there is no LO contribution. All results are given at the hadron level, i.e., the partonic cross sections are convoluted with the (anti)proton PDFs and the FF for $c \to D^{*+}$. We average over D^{*+} and D^{*-} mesons. We use the PDF set CTEQ6M [29] and the FF set obtained in Ref. [3] by fitting data from the OPAL Collaboration at NLO. Although the CTEQ6M PDFs were determined in the ZM-VFN scheme with $n_f = 5$, for the time being, we only include three light-quark flavors along with the gluon as incoming partons for all values of μ_F. Since, at this point, we wish to focus on effects related to the hard-scattering cross sections, the LO cross sections are evaluated using the same conventions concerning $\alpha_s(\mu_R)$, proton PDFs and $D^{*\pm}$ FF as in NLO. We consider $d\sigma/dp_T$ at $\sqrt{S} = 1.96$ TeV as a function of p_T with y integrated over the range $-1.0 < y < 1.0$. As for the QCD input parameters, we take the charm-quark mass to be $m = 1.5$ GeV and evaluate $\alpha_s^{(n_f)}(\mu_R)$ with $n_f = 4$ and asymptotic scale parameter $\Lambda^{(4)}_{\rm QCD} = 328$ MeV, which corresponds to $\alpha_s^{(5)}(m_Z) = 0.1181$. The renormalization scale μ_R and the factorization scales μ_F and μ_F' are set equal, $\mu_R = \mu_F = \mu_F'$. Details for the calculation of $d\sigma/dp_T$ from $d^2\sigma/dvdw$ have been given for direct $\gamma\gamma$ scattering in Eq. (45) of Ref. [16]. In this equation, the photon distribution functions must be replaced by the (anti)proton PDFs of the gluon and the light (anti)quarks.

The results for the gg channel are shown in Fig. 2. In Fig. 2(a), the renormalization and factorization scales are $\mu_R = \mu_F = \mu_F' = m$, but the scales in α_s, the PDFs and the FF are fixed at $2.1m$, to stay above the starting scale of the FF. The full line in Fig. 2(a) corresponds to the massless limit of the FFN calculation as derived in Sec. III A (σ_0), and the dashed curve is the result of the massive calculation (σ_m). We see that the massive cross section approaches the massless one very slowly at large values of p_T. At $p_T = 20$ GeV, the difference between the massive and massless cross sections is still of the order of 6%. The ratio R_{gg} for the massive cross section is always larger than its massless limit in the p_T range between 5 and 100 GeV. From this comparison, we conclude that, in the gg channel, the terms proportional to m^2/p_T^2 are particularly large and lead to an increase of the massive cross section as compared to the massless approximation. Similar observations were made

in Ref. [10], where the massive and massless calculations were compared as functions of the mass m for fixed value of p_T. For our application, we are interested in the massive and massless cross sections, where the finite Δc_i terms derived in Sec. III A are subtracted. This leads to the dashed-dotted (σ_m^Δ) and the dotted (σ_0^Δ) curves in Fig. 2(a). We have checked that our result for the massless calculation after subtraction, i.e., the dotted curve, is in perfect agreement with the results in the ZM-VFN scheme obtained using the FORTRAN program of Refs. [3,21]. This comparison demonstrates that the finite Δc_i terms, which, if subtracted, should produce the ZM-VFN cross section, are correct. Their subtraction from the FFN result will give the GM-VFN result, which approaches the ZM-VFN result at large values of p_T. We see that the contribution of these finite terms is by no means negligible.

The ratios plotted in Fig. 2(a) show that, in the low- to medium-p_T range, the NLO cross section is up to a factor of about 5 larger than the LO one (note that the numerator of R_{gg} is the sum of the LO result and the NLO corrections). This is not surprising, since we have chosen very low values for the renormalization and factorization scales. Since we are interested in the region where $p_T \gtrsim m$, a better choice of scales is $\mu \approx p_T$. As usual, we choose

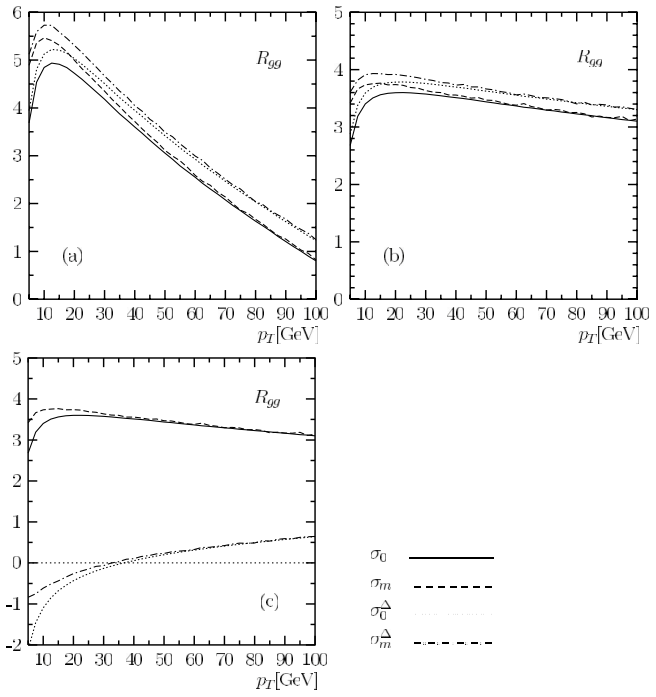

FIG. 2. gg contribution to $p + \bar{p} \to D^{*\pm} + X$ including Abelian and non-Abelian parts, normalized to the LO cross section with $m = 0$. (a) Renormalization and factorization scales are $\mu_R = \mu_F = \mu_F' = m$ (but fixed at $2.1m$ in α_s, PDFs and FF). (b) Same as in part (a), but for $\mu_R = \mu_F = \mu_F' = 2m_T$ including rescaling due to renormalization and initial-state factorization of singularities originating from internal gluons. (c) Same as in part (a), but including full rescaling to $\mu_R = \mu_F = \mu_F' = 2m_T$.

$\mu_R = \mu_F = \mu_F' = 2m_T$, which can be used for both small and large values of p_T. To obtain the cross sections at this scale, we must add the terms proportional to $\ln(m^2/\mu^2)$ as described in Sec. III A in the massless limit and the corresponding terms for the FFN scheme contained in Ref. [7]. In Fig. 2(b), we first show the results for the cross section ratios including the rescaling due to renormalization and initial-state factorization, i.e., adding Eq. (27) using the coefficients of Eqs. (28)–(31) for the massless calculation and the corresponding mass-dependent terms of Ref. [7] for the massive calculation. As in Fig. 2(a), we show four curves corresponding to the massive and massless calculations, in either case without and with finite terms subtracted. In this case, the cross section ratios exhibit a much weaker p_T dependence. The QCD correction (K) factor is somewhat smaller now, but it is still large, showing that the perturbative expansion for the gg channel is not converging very well. We observe that the massive cross sections converge to the corresponding massless cross sections with increasing value of p_T as in Fig. 2(a). The effect of the subtraction of the finite terms is slightly smaller, since the added $\ln(\mu^2/m^2)$ terms apparently have smaller m^2/p_T^2 corrections. The curves for the massive theory lie always above the massless approximation, as in Fig. 2(a).

If it were not for the choice $n_f = 4$ in α_s and the fact that the CTEQ6M proton PDFs are evolved according to the ZM-VFN scheme, so that the charm and bottom PDFs participate in the DGLAP evolution for sufficiently high values of μ_F, the unsubtracted result σ_m in Fig. 2(b) would correspond to the cross section in the genuine FFN scheme. We have seen that this theory is characterized by large NLO corrections. This has its origin in the fact that the contributions of the would-be collinear divergences related to incoming and outgoing charm-quark lines are not yet subtracted, i.e., they are still left at the factorization scales $\mu_F = \mu_F' = m$. It is clear that these contributions must be also evaluated at the factorization scales $\mu_F = \mu_F' = 2m_T$, since our FF for $c \to D^{*+}$ is evolved to this scale and we want to include the contributions from the charm content of the incoming (anti)proton. To do this, we must include the additional contributions proportional to $\ln(\mu_R^2/m^2)$, $\ln(\mu_F^2/m^2)$ and $\ln(\mu_F'^2/m^2)$ in Eqs. (35)–(40). The result is shown in Fig. 2(c). The subtracted massive calculation (σ_m^Δ) is represented by the dashed-dotted curve and the result of the subtracted massless calculation (σ_0^Δ) by the dotted one. The latter curve again agrees with the ZM-VFN result calculated on the basis of Ref. [20]. For comparison, we also show the results for σ_0 and σ_m from Fig. 2(b) before the additional logarithmic terms from Eqs. (35)–(40) are subtracted, and also without subtraction of the finite Δc_i terms. The lower two curves are our final results for the gg channel. The cross section ratios are negative for $p_T \lesssim 30$ GeV and rise up to approximately 0.6 at $p_T = 100$ GeV. The massive cross section approaches its massless limit with increasing value of p_T. As we shall see later,

the gg channel is only important at small values of p_T; at higher values of p_T, the total cross section is dominated by the contribution due to the charm content of the (anti)proton. Since this dominating contribution does not contain finite-m corrections, the effect of mass-dependent terms in the gg channel will be suppressed in the final result.

In Fig. 3, we present results for the $q\bar{q}$ channel. The cross section ratios shown here are normalized to the corresponding LO cross section for the $q\bar{q}$ initial states. Since this normalization differs from the LO gg cross section, the ratios in Figs. 2 and 3 should not be added. In Fig. 3(a), the ratios with the renormalization and factorization scales equal to m are shown. The massless and massive cross sections, i.e., the full (σ_0) and the dashed (σ_m) curves with no subtraction of finite terms and the dotted (σ_0^Δ) and dashed-dotted (σ_m^Δ) curves with Δc_i terms subtracted, almost coincide. This means that, for the $q\bar{q}$ channel, the m^2/p_T^2 terms are negligibly small in the considered p_T range. We notice that the NLO cross section for this channel is negative, except for small values of p_T. The subtraction terms are non-negligible over the whole p_T range. In Fig. 3(b), the cross section ratio at the scale $\mu_R = \mu_F = \mu_F' = 2m_T$ including the rescaling due to renormalization and initial-state factorization according to Eqs. (27) and (55)–(58) is shown. At this scale, the cross section is positive for all p_T values. The influence of the m^2/p_T^2 terms is somewhat larger now due to additional mass-dependent contributions in the terms proportional to $\ln(\mu^2/m^2)$. Also the difference due to the subtraction of the finite Δc_i terms is larger, since the PDFs and the FF are evaluated at much larger scales. We note that the massive ratio is smaller than the massless one. If the logarithmic rescaling terms due to internal charm-quark lines in Eqs. (34) and (59)–(62) are subtracted, we obtain the cross section ratios presented in Fig. 3(c). These results are needed in our final analysis. The dashed-dotted (σ_m^Δ) and dotted (σ_0^Δ) curves lie very near to each other showing that the m^2/p_T^2 terms are much smaller in this channel. Also in this case, we checked that our result for the massless calculation with subtraction and rescaling included agrees perfectly with the ZM-VFN result of Ref. [20]. For comparison, the unsubtracted massive (σ_m) and massless (σ_0) results from Fig. 3(b) are again shown in Fig. 3(c). In contrast to the gg channel, the last rescaling due to singular internal charm-quark lines leads to an increased ratio.

Finally, we discuss the m^2/p_T^2 contributions for the gq and $g\bar{q}$ channels. For definiteness, we consider the $p(q) + \bar{p}(g)$ contributions to $p + \bar{p} \to D^{*\pm} + X$ separately for the cases where the $D^{*\pm}$ meson originates from a charm or an anticharm quark. We normalize the cross sections to the LO gg-channel cross section. Using as scales m in the same way as in Fig. 2(a), we obtain the full and dashed curves in Fig. 4(a) corresponding to massless (σ_0) and massive (σ_m) cross sections, respectively. The upper curves are for observed anticharm and the lower ones for

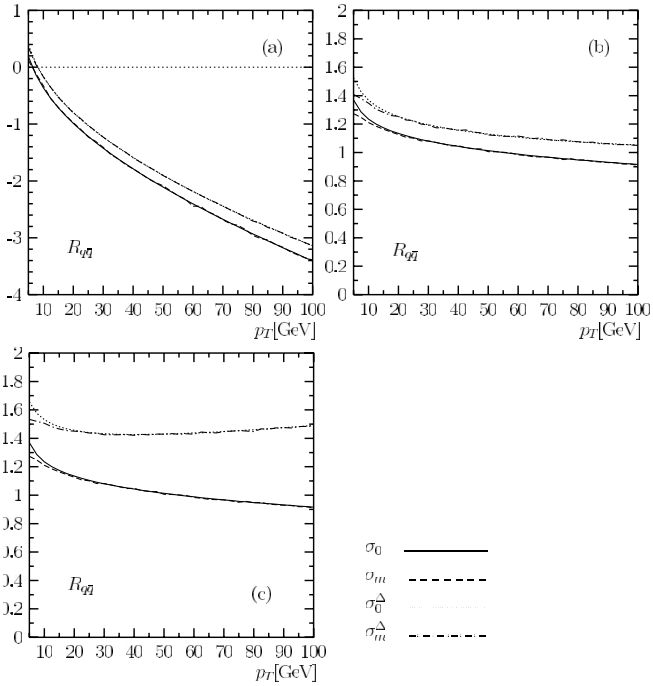

FIG. 3. $p(q) + \bar{p}(\bar{q})$ contribution to $p + \bar{p} \to D^{*\pm} + X$ including Abelian and non-Abelian parts, normalized to the LO cross section with $m = 0$. (a) Renormalization and factorization scales are $\mu_R = \mu_F = \mu_F' = m$ (but fixed at $2.1m$ in α_s, PDFs and FF). (b) Same as in part (a), but for $\mu_R = \mu_F = \mu_F' = 2m_T$ including rescaling due to renormalization and initial-state factorization. (c) Same as in part (a), but including full rescaling to $\mu_R = \mu_F = \mu_F' = 2m_T$.

observed charm. These two sets of curves differ only little. The m^2 power corrections are small over the whole p_T range. If we rescale to the scale $2m_T$ using Eqs. (27), (66) and (67), we obtain the massless (full curves) and massive (dashed curves) results for observed charm in Fig. 4(b) and those for observed anticharm in Fig. 4(c). Here, the ratio of cross sections is positive. We observe that the massive cross section is slightly larger than the massless one. If we include the full rescaling of logarithmic terms due to charm or anticharm exchange using Eqs. (27) and (34) with Eqs. (66)–(70), we obtain the lower curves in Fig. 4(b) and 4(c), respectively, for the massive (dashed-dotted curves) and massless (dotted curves) cross sections. The latter ones are again in perfect agreement with the ZM-VFN results of Ref. [20]. These results will be used for the final cross section.

So far, we have only considered the channels with gluon or light (anti)quarks in the initial state and (anti)charm quarks in the final state. To these contributions, we must add the cross sections with (anti)charm quarks in the initial state. Such results will be shown in the next three figures. From Figs. 2(c), 4(b) and 4(c), we see that the gg and gq channels yield negative contributions (for $p_T < 30$ GeV in the gg case and for all values of p_T in the gq case), while only the $q\bar{q}$ channel gives a positive contribution every-

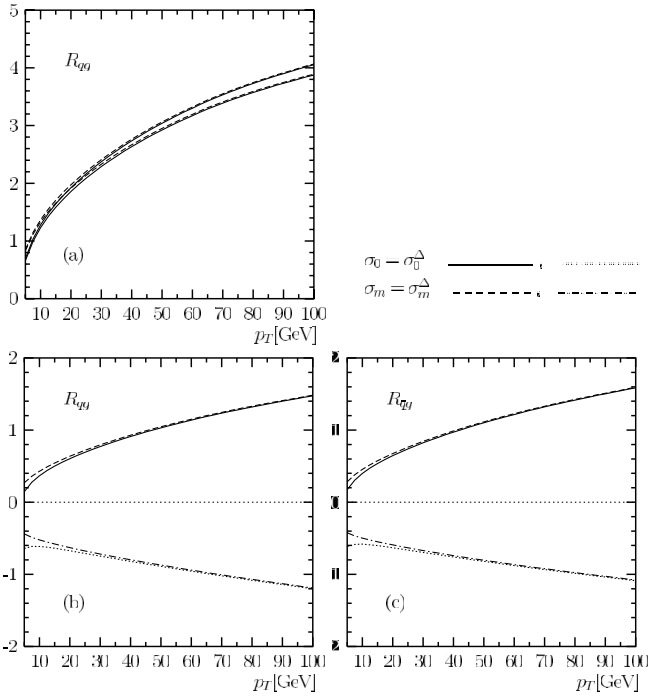

FIG. 4. (a) $p(q) + \bar{p}(g)$ contribution to $p + \bar{p} \to D^{*\pm} + X$ including Abelian and non-Abelian parts, normalized to the LO cross section of the gg channel with $m = 0$. Renormalization and factorization scales are $\mu_R = \mu_F = \mu_F' = m$ (but fixed at $2.1m$ in α_s, PDFs and FF). Lower curves: observed charm, upper curves: observed anticharm. (b) Same as in part (a) for observed charm, but with renormalization and factorization scales chosen as $\mu_R = \mu_F = \mu_F' = 2m_T$. (c) Same as in part (b), but for observed anticharm.

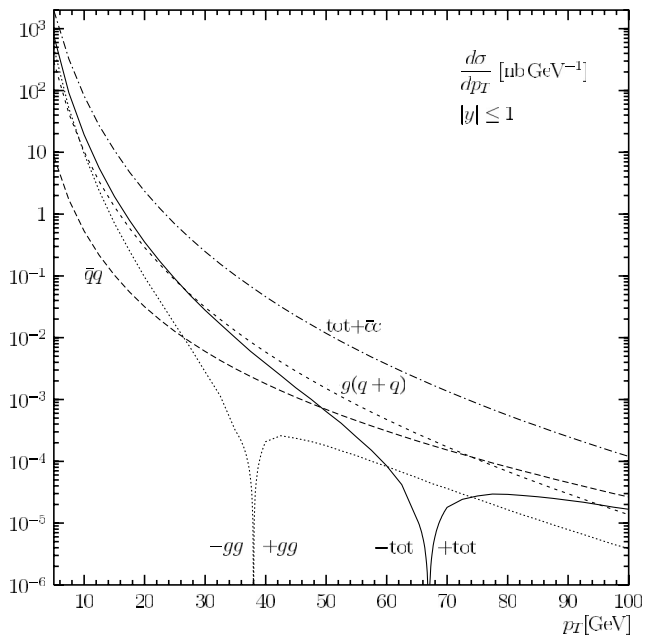

FIG. 5. Partial cross sections for $p + \bar{p} \to D^{*\pm} + X$, averaged over D^{*+} and D^{*-} mesons, in the ZM-VFN scheme. Renormalization and factorization scales are $\mu_R = \mu_F = \mu_F' = 2m_T$. The sum of the gg, $q\bar{q}$, gq and $g\bar{q}$ channels is labeled tot, the total cross section including incoming (anti)charm quarks tot + $c\bar{c}$.

where. Their sum is still negative for $p_T < 65$ GeV, as can be seen in Fig. 5, where we have plotted the sum of these three channels as the solid curve labeled tot. Only when the contributions from incoming (anti)charm quarks are added, we obtain, as a meaningful result, a positive cross section, which is shown in Fig. 5 as the dashed-dotted curve labeled tot + $c\bar{c}$. These results are for the subtracted massless approach (σ_0^Δ) and represent the cross section for inclusive $D^{*\pm}$ production, including only the contribution due to the fragmentation of a (anti)charm quark, but not the ones due to the fragmentation of a gluon or a light (anti)quark. In addition to these results, we also show in Fig. 5 the partial cross sections for the gg, $q\bar{q}$ and $g(q + \bar{q})$ channels. The latter channel contains all contributions with a gluon and a light (anti)quark coming from the (anti)proton. We see that the sum of all components yields a cross section with a smooth, steeply falling p_T dependence. The comparison with the equivalent results with massive (anti)charm quarks is made in Fig. 6, where we show for each partial result the ratio with respect to the full result including the contribution from c ($\bar{c}$) initial states. The upper and lower curves correspond to the subtracted massive (σ_m^Δ) and massless (σ_0^Δ) calculations, respectively. As we can see, the m^2/p_T^2 corrections in the sum of all contributions with gluons or light (anti)quarks in the initial state labeled tot are modest, except at small values of p_T. At the smallest p_T value considered, $p_T = 5$ GeV, the massless cross section is only increased by roughly 20% when these corrections are included, although the contribution labeled tot is substantially increased, from -773 nb GeV^{-1} for the massless calculation to -386 nb GeV^{-1} for the massive one. We emphasize that all results in Figs. 5 and 6 refer to the scale choice $\mu_R = \mu_F = \mu_F' = 2m_T$.

IV. COMPARISON WITH CDF DATA

Before we can compare our final results with experimental data, we have to add another contribution, which was not yet discussed, but is non-negligible for the experimental situation at the Tevatron: in fact, the observed $D^{*\pm}$ meson may also be produced through the fragmentation of a gluon or a light (anti)quark. Appropriate $g, q, \bar{q} \to D^{*\pm}$ FFs are contained in the OPAL set of Ref. [3], where they are generated via NLO evolution assuming that they vanish at the starting scale. In the ZM-VFN scheme, gluon and light (anti)quark fragmentation already contributes at LO. By contrast, these types of contribution do not exist in the FFN scheme, where the collinear $g \to c\bar{c}$ splitting is treated perturbatively instead, starting only in NLO. Since the GM-VFN scheme is to be constructed in such a way that it merges with the ZM-VFN scheme at large

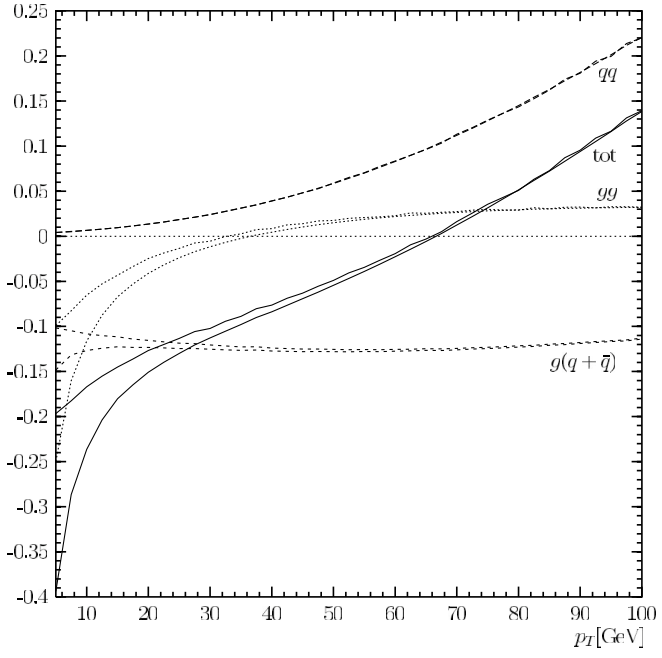

FIG. 6. Partial cross sections normalized to the result for all contributions including the $c\bar{c}$ initial state. Lower and upper curves correspond to the massless and massive calculations, respectively.

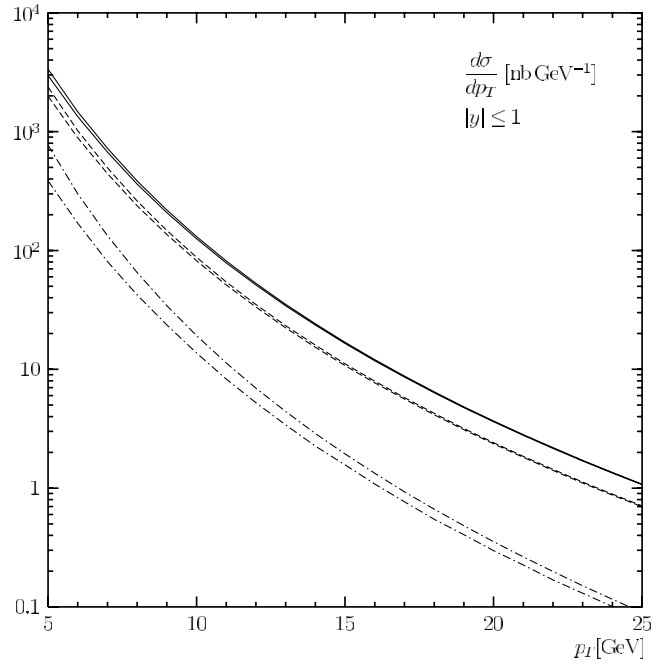

FIG. 7. p_T spectrum for $p + \bar{p} \to D^{*\pm} + X$, averaged over D^{*+} and D^{*-} mesons, including all contributions. Renormalization and factorization scales are $\mu_R = \mu_F = \mu_F' = 2m_T$. Dashed-dotted lines: the (negative) contributions with gluons and light (anti)quarks in the initial state; dashed lines: including (anti)charm quarks in the initial state; full lines: including the contribution from $g, q, \bar{q} \to D^{*\pm}$ fragmentation. Upper and lower curves correspond to the massive and massless calculations, respectively.

values of p_T, it is clear that the gluon and light (anti)quark fragmentation contributions must be accommodated in the GM-VFN framework as well. A certain part of these contributions carries mass dependence, because of internal charm-quark lines and external ones that do not lead to fragmentation. In the FFN scheme, the analogous mass dependence only comes in beyond NLO. Therefore, we ignore this mass dependence for the time being and adopt the gluon and light (anti)quark fragmentation contributions from the ZM-VFN analysis [20]. These contributions amount to slightly more than 30%, almost independent of p_T, as can be seen in Fig. 7. The bulk is due to gluon fragmentation. For photoproduction in ep and $\gamma\gamma$ collisions, this contribution was found to be negligible [16–18].

The effect of mass-dependent terms is very much reduced in the final cross section, since the parts which have to be calculated with $m = 0$ are large. Therefore, one cannot expect that mass terms would increase the theoretical predictions towards cross sections as high as observed in the CDF experiment [1]. The size of the mass-dependent terms is visualized in Fig. 8, where we show the ratios of cross sections calculated with $m \neq 0$ to those with $m = 0$. For the (negative) contributions due to incoming gluons and light (anti)quarks, mass-dependent terms lead to a reduction in size by 50% at $p_T = 5$ GeV. At this value of p_T, the ratio of massive over massless results is reduced to 1.19 and 1.13 when the contributions from incoming (anti)charm quarks and from $g \to D^{*\pm}$ fragmentation, respectively, are included.

Since the effect of mass-dependent terms is very much reduced in the final cross section, it is clear that a variation of the value of the charm-quark mass does not contribute much to the theoretical uncertainty. Whereas the sum of the contributions due to gluons and light (anti)quarks in the initial state varies by -20.5% ($+17.8\%$) at $p_T = 5$ GeV if m is changed from our default value of 1.5 to 1.2 (1.8) GeV, the cross section also including those terms which can be calculated in the massless approach only [i.e., those with (anti)charm quarks in the initial state and from $g, q, \bar{q} \to D^{*\pm}$ fragmentation] varies by only -2.5% ($+1.8\%$). The theoretical uncertainty is, therefore, dominated by the choice of the renormalization and factorization scales. The results presented in Fig. 7 were obtained for $\mu_R = \mu_F = \mu_F' = 2m_T$. A conservative mode of scale variation frequently encountered in the literature is to independently vary the values of μ_R/m_T, μ_F/m_T and μ_F'/m_T between $1/2$ and 2 about the default value 1. We will adopt this prescription for the comparison with experimental data from the CDF Collaboration [1]. This leads to large changes at $p_T = 5$ GeV (for the massless calculation in the range between -41% and $+30\%$, and for the massive calculation between -46% and $+56\%$). At $p_T = 25$ GeV, the variations are smaller and cover the range $\pm 20\%$. Minimal values for $d\sigma/dp_T$ are obtained for maxi-

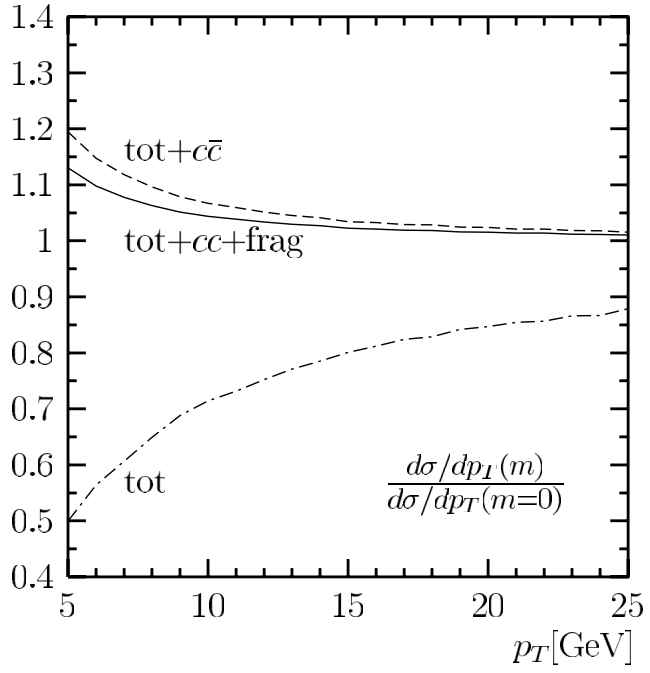

FIG. 8. Ratios of the subtracted massive and massless differential cross sections $d\sigma/p_T$ for $p + \bar{p} \to D^{*\pm} + X$ with $|y| \leq 1$ including (a) all contributions (full line), (b) all contributions with incoming gluons, light (anti)quarks and (anti)charm quarks, but without the $g, q, \bar{q} \to D^{*\pm}$ fragmentation contributions (dashed line), and (c) the sum of the contributions with only gluons and light (anti)quarks in the initial state (dashed-dotted line). Renormalization and factorization scales are $\mu_R = \mu_F = \mu_F' = 2m_T$.

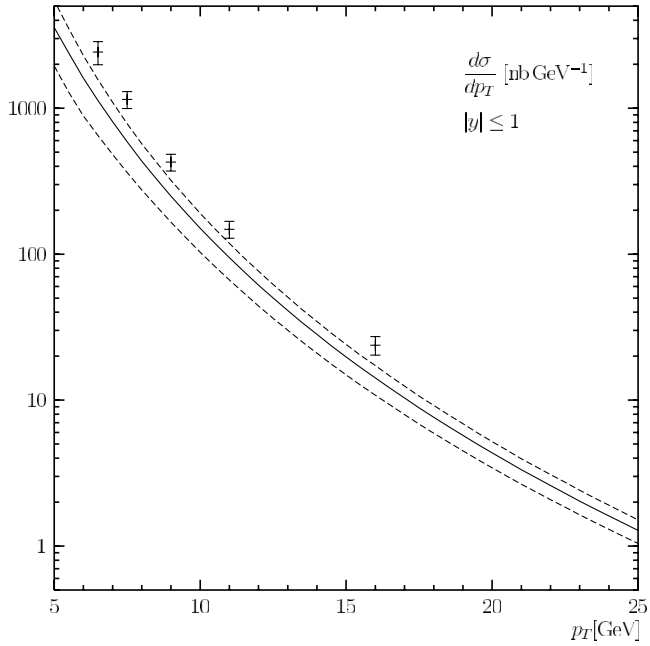

FIG. 9. Variation of the p_T spectrum of $p + \bar{p} \to D^{*\pm} + X$, averaged over D^{*+} and D^{*-} mesons, with the renormalization and factorization scales in the GM-VFN scheme. The central solid curve is for $\mu_R = \mu_F = \mu_F' = m_T$, the upper and lower dashed curves represent the maximum and minimum cross sections found by varying μ_R, μ_F and μ_F' independently within a factor of 2 up and down relative to the central values. The contributions from (anti)charm quarks in the initial state and from $g, q, \bar{q} \to D^{*\pm}$ fragmentation are included. The data points are from the CDF Collaboration [1].

mal values of μ_R and μ_F' and minimal value of μ_F, and maximum values are reached for minimal values of μ_R and μ_F' and maximal value of μ_F. These results are presented in Fig. 9 as a band of predicted values. A comparison with experimental data from CDF [1], also shown in this figure, shows that the data prefer a small renormalization scale and a large initial-state factorization scale. However, even for the choice $\mu_R = m_T/2$ and $\mu_F = 2m_T$, the theoretical results in the GM-VFN scheme still undershoot the measured cross sections by 20% to 34%.

Residual sources of theoretical uncertainty include the variations in the available PDF and FF sets. The new generation of NLO proton PDF sets exhibit only minor differences. Similarly, the two NLO FF sets that were determined in Ref. [3] by fitting slightly incompatible data from the ALEPH and OPAL Collaborations yield rather similar predictions, the difference being of order 10% or less in the kinematic range of the CDF data [1]. The inclusion of these additional errors would broaden the theoretical error band in Fig. 9 only insignificantly.

We stress that our results do not include a contribution due to bottom-quark production. This part can be identified in the experimental analysis and was, in fact, removed from the CDF data shown in Fig. 9.

V. SUMMARY AND CONCLUSIONS

In this work, we calculated the NLO corrections to inclusive charm production in $p\bar{p}$ collisions in two approaches using massive or massless charm quarks. By deriving the massless limit from the massive theory (FFN scheme), we could show that this limit differs from the genuine massless version with $\overline{\text{MS}}$ factorization (ZM-VFN scheme) by finite corrections. We adjusted subtraction terms and thus managed to establish a massive theory with $\overline{\text{MS}}$ subtraction (GM-VFN scheme) which approaches the massless theory (ZM-VFN scheme) with increasing transverse momentum. With these results and including the contributions where a (anti)charm quark occurs as an incoming parton and those where a gluon or light (anti)-quark fragments, we calculated the inclusive $D^{*\pm}$ cross section in $p\bar{p}$ collisions at $\sqrt{S} = 1.96$ TeV using realistic nonperturbative FFs, which are subject to proper DGLAP evolution [13] and manifestly universal [14]. Our central prediction somewhat undershoots a recent measurement by the CDF Collaboration [1], but reasonable agreement can be reached by adjusting the renormalization and factorization scales within a plausible range of tolerance.

We made the observation that, in contrast to other experimental situations such as $\gamma\gamma$ or γp collisions, the contribution from $g \to D^{*\pm}$ fragmentation is large. The FFs which we used here had been obtained from fits to data from the CERN LEP. One may speculate, therefore, whether these data leave enough room to adjust the $g \to D^{*\pm}$ FF and improve the agreement with the Tevatron data. We plan to come back to this question in a future publication.

ACKNOWLEDGMENTS

We are grateful to I. Bojak for providing his NLO FORTRAN code for the hadroproduction of heavy flavors and for clarifying comments, and to S. Kretzer for useful discussions. The work of I. Schienbein was supported by DESY. This work was supported by the Bundesministerium für Bildung und Forschung through Grant No. 05 HT4GUA/4.

APPENDIX A: COEFFICIENTS FOR SUBPROCESS $g + g \to c + X$

In this appendix, we list the coefficients c_i needed for the calculation of the cross section for the inclusive production of charm in gg collisions. They are obtained by taking the limit $m \to 0$ of the cross sections calculated in Ref. [7]. These limits are compared with the results from Ref. [20] in order to obtain the subtraction terms Δc_i. To shorten the expressions, we make use of the abbreviations

$$X = 1 - vw, \quad Y = 1 - v + vw, \quad v_i = i - v, \tag{A1}$$

and write down only nonzero contributions. The coefficients given below have to be used together with Eqs. (12) and (20); their color decomposition is defined in Eq. (16). We start with the Abelian coefficients $c_i^{\rm qed}$.

1. $c_i^{\rm qed}$ coefficients

$$\begin{aligned}
c_1^{\rm qed} &= \frac{-21 - 6\ln v + 9\ln^2 v + 3\ln v_1 + 3\ln^2 v_1 + 4\pi^2}{6}\tau(v) + \frac{5\ln v_1 + \ln^2 v_1 - \ln v + 3\ln^2 v}{2v_1} \\
&\quad + \frac{5\ln v + \ln^2 v - \ln v_1 + 3\ln^2 v_1}{2v} + \Delta c_1^{\rm qed}, \quad \Delta c_1^{\rm qed} = 2(1 - \ln v - \ln^2 v)\tau(v), \quad \tilde{c}_1^{\rm qed} = -\frac{1}{2}(3 + 4\ln v)\tau(v), \\
c_2^{\rm qed} &= \frac{1}{2}(4\ln v - 3)\tau(v) + \Delta c_2^{\rm qed}, \quad \Delta c_2^{\rm qed} = -2(1 + 2\ln v)\tau(v), \quad \tilde{c}_2^{\rm qed} = -2\tau(v), \quad c_3^{\rm qed} = 2\tau(v) + \Delta c_3^{\rm qed}, \\
\Delta c_3^{\rm qed} &= -4\tau(v), \quad c_5^{\rm qed} = \frac{-2(1+2v^2)}{v} + \frac{3 - 2v + 2v^2}{vw} - \frac{2(-1 + v - v^2 + 2v^3)w}{v_1 v} - \frac{2(-v + v^2)}{X^3} - \frac{2v}{X^2} + \frac{3v - 4v^2 + 2v^3}{v_1 X} \\
&\quad - \frac{2v}{Y} + \Delta c_5^{\rm qed}, \quad \Delta c_5^{\rm qed} = \frac{2v}{v_1} - \frac{2(2 - 2v + v^2)}{vw} + \frac{2v^2 w}{v_1} + \frac{4v}{Y}, \quad c_6^{\rm qed} = \frac{-4v^2}{v_1} + \frac{2(-2 + 5v - 3v^2 + 2v^3)}{v_1 vw} + \frac{2v^2 w}{v_1}, \\
c_7^{\rm qed} &= \frac{-2}{vw} - \frac{4v}{Y}, \quad c_8^{\rm qed} = \frac{2(2 - 2v + v^2)}{vw}, \quad c_9^{\rm qed} = \frac{-2v}{v_1} + \frac{2}{vw} - \frac{2v^2 w}{v_1}, \\
c_{10}^{\rm qed} &= \frac{2(-1 + v - 2v^2 + 4v^3)}{v_1 v} - \frac{-3 + 7v - 4v^2 + 4v^3}{v_1 vw} - \frac{2(-1 + v - v^2 + 3v^3)w}{v_1 v} + \frac{2(v - v^2)}{X^3} \\
&\quad - \frac{2v}{X^2} + \frac{3v - 4v^2 + 2v^3}{v_1 X} - \frac{2v}{Y} + \Delta c_{10}^{\rm qed}, \quad \Delta c_{10}^{\rm qed} = \Delta c_5^{\rm qed}, \\
c_{11}^{\rm qed} &= \frac{7 - 8v + 6v^2 - 4v^3}{v_1 v} + \frac{1 - 2v + 4v^2}{2vw} + \frac{(-8 + 8v - 3v^2 + v^3)w}{v_1 v} - \frac{8v_1 v}{X^3} + \frac{7v}{X^2} + \frac{v_2(-v + 3v^2)}{v_1 X} + \frac{2v}{Y} + \Delta c_{11}^{\rm qed}, \\
\Delta c_{11}^{\rm qed} &= \frac{1}{2}\Delta c_{10}^{\rm qed}, \quad \tilde{c}_{11}^{\rm qed} = \frac{2(1+2v^2)}{v} + \frac{-3 + 2v - 2v^2}{vw} + \frac{2(-1 + v - v^2 + 2v^3)w}{v_1 v} - \frac{2vv_1}{X^3} + \frac{2v}{X^2} + \frac{-3v + 4v^2 - 2v^3}{v_1 X} + \frac{2v}{Y}, \\
c_{12}^{\rm qed} &= -4 - \frac{2}{v_1} - \frac{2}{v}, \quad c_{13}^{\rm qed} = -2 + \frac{4}{v_1} + \frac{2}{v}, \quad c_{14}^{\rm qed} = -2 + \frac{2}{v_1} + \frac{4}{v}.
\end{aligned} \tag{A2}$$

We note that these results for the Abelian part agree with the coefficients for $\gamma + \gamma \to c + X$ in Ref. [16], if the normalization factor $C(s)$ in Ref. [16] is replaced by $C(s) = 1$. In that work, the zero-mass limit was derived from the FFN cross sections of Ref. [30] and compared with the ZM-VFN ones of Ref. [27].

2. c_i^{oq} coefficients

$$
\begin{aligned}
c_1^{\mathrm{oq}} &= \Bigg[\frac{-1+7\ln v+16\ln^2 v+2\ln v_1-16\ln v\ln v_1+4\ln^2 v_1}{2}\\
&\quad-\frac{(-30-3\ln v+120\ln^2 v-15\ln v_1-96\ln v\ln v_1+36\ln^2 v_1+8\pi^2)v}{6}\\
&\quad+\frac{(-15-9\ln v+42\ln^2 v-24\ln v\ln v_1+12\ln^2 v_1+4\pi^2)v^2}{3}\Bigg]\tau(v)\\
&\quad-\frac{-1+2\ln v+4\ln^2 v+7\ln v_1}{2v_1}+\frac{1-7\ln v-2\ln v_1-4\ln^2 v_1}{2v}+\Delta c_1^{\mathrm{oq}},\quad \Delta c_1^{\mathrm{oq}}=4(-1+\ln v+\ln^2 v)v_1 v\tau(v),\\
\tilde{c}_1^{\mathrm{oq}} &= [-4(\ln v-\ln v_1)+(3+12\ln v-8\ln v_1)v-(3+12\ln v-8\ln v_1)v^2]\tau(v),\\
c_2^{\mathrm{oq}} &= [-8(-2\ln v+\ln v_1)+(3-36\ln v+16\ln v_1)v-(3-28\ln v+8\ln v_1)v^2]\tau(v)+\Delta c_2^{\mathrm{oq}},\quad \Delta c_2^{\mathrm{oq}}=4(1+2\ln v)vv_1\tau(v),\\
\tilde{c}_2^{\mathrm{oq}} &= (-8+20v-20v^2)\tau(v),\quad c_3^{\mathrm{oq}}=4(4-9v+9v^2)\tau(v)+\Delta c_3^{\mathrm{oq}},\quad \Delta c_3^{\mathrm{oq}}=8v_1 v\tau(v),\\
c_5^{\mathrm{oq}} &= \frac{-2(-2+12v-30v^2+81v^3-81v^4+32v^5)}{v_1^2 v}+\frac{8(4-13v+20v^2-14v^3+4v^4)}{v_1 vw^2}\\
&\quad+\frac{2(4+19v-112v^2+189v^3-128v^4+32v^5)}{v_1^2 vw}+\frac{4(-1+6v-12v^2+43v^3-52v^4+28v^5)w}{v_1^2 v}-\frac{48v^4w^2}{v_1^2}\\
&\quad+\frac{32v^4w^3}{v_1^2}-\frac{4v_1 v}{X^3}+\frac{4v(5-4v)}{X^2}-\frac{4(-3v+13v^2-13v^3+4v^4)}{v_1 X}+\frac{4v_1^2 v}{Y^3}\\
&\quad-\frac{4v_1 v(6-5v)}{Y^2}-\frac{2(-5v-4v^2+4v^3)}{Y}+\Delta c_5^{\mathrm{oq}},\quad \Delta c_5^{\mathrm{oq}}=-4v+\frac{8vv_1^2}{Y^3}-\frac{8v^2v_1}{Y^2}+\frac{4v(3-6v+4v^2)}{Y},\\
c_6^{\mathrm{oq}} &= \frac{2v(13-5v+8v^2)}{v_1^2}-\frac{8(1-2v+2v^2)}{v_1 vw^2}+\frac{4(-1-2v+10v^2-13v^3+4v^4)}{v_1^2 vw}-\frac{8v^2(11-11v+8v^2)w}{v_1^2}\\
&\quad+\frac{32v^3(1+v)w^2}{v_1^2}-\frac{32v^4w^3}{v_1^2},\\
c_7^{\mathrm{oq}} &= \frac{6v(-7+6v)}{v_1}-\frac{2(-1+4v)}{w}+\frac{8v^2w}{v_1}+\frac{8vv_1^2}{Y^3}-\frac{8(6v-11v^2+5v^3)}{Y^2}+\frac{4(25v-18v^2+4v^3)}{Y},\\
c_8^{\mathrm{oq}} &= \frac{-2v(6+17v-27v^2+16v^3)}{v_1^2}+\frac{8(1-2v+2v^2)}{v_1w^2}+\frac{8(1-v+v^3)}{v_1^2w}+\frac{4v(4+15v-27v^2+20v^3)w}{v_1^2}\\
&\quad-\frac{48v^4w^2}{v_1^2}+\frac{32v^4w^3}{v_1^2}-\frac{4(7v-8v^2+4v^3)}{X}+\frac{12v_1 v}{Y},\\
c_9^{\mathrm{oq}} &= \frac{-2(6-25v+76v^2-77v^3+32v^4)}{v_1^2}+\frac{8(2-7v+12v^2-10v^3+4v^4)}{v_1 vw^2}+\frac{2(2+9v-54v^2+101v^3-78v^4+24v^5)}{v_1^2 vw}\\
&\quad+\frac{8v^2(9-11v+6v^2)w}{v_1^2}-\frac{16v^2(1-v+v^2)w^2}{v_1^2}+\frac{4(5v-8v^2+4v^3)}{v_1 X}-\frac{12v_1 v}{Y},\\
c_{10}^{\mathrm{oq}} &= \frac{2(2-6v+11v^2-47v^3+48v^4-16v^5)}{v_1^2 v}+\frac{8(3-10v+16v^2-12v^3+4v^4)}{v_1 vw^2}\\
&\quad+\frac{2(4+11v-76v^2+135v^3-94v^4+24v^5)}{v_1^2 vw}+\frac{4(-1+6v-12v^2+41v^3-50v^4+24v^5)w}{v_1^2 v}\\
&\quad-\frac{16v^2(-1+v+2v^2)w^2}{v_1^2}+\frac{32v^4w^3}{v_1^2}-\frac{4vv_1}{X^3}-\frac{4v(-5+4v)}{X^2}-\frac{4(2v+5v^2-9v^3+4v^4)}{v_1 X}+\frac{4vv_1^2}{Y^3}\\
&\quad+\frac{4v_1 v(-6+5v)}{Y^2}-\frac{2v(-11+2v+4v^2)}{Y}+\Delta c_{10}^{\mathrm{oq}},\quad \Delta c_{10}^{\mathrm{oq}}=\Delta c_5^{\mathrm{oq}},
\end{aligned}
$$

$$
\begin{aligned}
c_{11}^{\mathrm{oq}} &= \frac{-10+33v-26v^2+57v^3-94v^4+48v^5}{v_1^2 v}+\frac{8(3-4v+2v^2)}{w^2}-\frac{2(-1+14v-30v^2+16v^3)}{vw}\\
&\quad-\frac{2(-6+21v-23v^2+41v^3-61v^4+32v^5)w}{v_1^2 v}+\frac{16v^3(-1+2v)w^2}{v_1^2}-\frac{16v^4w^3}{v_1^2}+\frac{12v_1 v}{X^3}+\frac{2v(-14+9v)}{X^2}\\
&\quad+\frac{13v-9v^2-2v^3}{v_1 X}-\frac{16v_1^2 v}{Y^3}+\frac{4v_1 v(13-9v)}{Y^2}+\frac{-65v+56v^2-10v^3}{Y}+\Delta c_{11}^{\mathrm{oq}}, \qquad \Delta c_{11}^{\mathrm{oq}}=\frac{1}{2}\Delta c_{10}^{\mathrm{oq}},\\
\tilde{c}_{11}^{\mathrm{oq}} &= \frac{2(-2+12v-26v^2+69v^3-73v^4+32v^5)}{v_1^2 v}-\frac{8(2-7v+12v^2-10v^3+4v^4)}{v_1 v w^2}\\
&\quad-\frac{2(17-68v+113v^2-82v^3+24v^4)}{v_1^2 w}+\frac{4(1-6v+12v^2-43v^3+52v^4-28v^5)w}{v_1^2 v}+\frac{48v^4w^2}{v_1^2}-\frac{32v^4w^3}{v_1^2}\\
&\quad+\frac{4v_1 v}{X^3}+\frac{4v(-5+4v)}{X^2}+\frac{4v(9-10v+3v^2)}{v_1 X}-\frac{4v_1^2 v}{Y^3}+\frac{4v_1 v(6-5v)}{Y^2}-\frac{2(25v-18v^2+4v^3)}{Y},\\
c_{12}^{\mathrm{oq}} &= 16(1-v+v^2), \qquad c_{13}^{\mathrm{oq}}=-16+24v-16v^2-\frac{4}{v_1}+\frac{4}{v}, \qquad c_{14}^{\mathrm{oq}}=-32+40v-32v^2+\frac{4}{v_1}+\frac{4}{v}.
\end{aligned}
\tag{A3}
$$

3. c_i^{kq} coefficients

$$
\begin{aligned}
c_1^{\mathrm{kq}} &= \left[\frac{-1-7\ln v-17\ln^2 v-6\ln v_1+16\ln v\ln v_1}{2}+\frac{(-54-15\ln v+15\ln^2 v-3\ln v_1-3\ln^2 v_1+8\pi^2)v}{6}\right.\\
&\quad\left.-\frac{(-27-9\ln v+6\ln^2 v+4\pi^2)v^2}{3}\right]\tau(v)+\frac{1+7\ln v_1+\ln^2 v_1+6\ln v+8\ln^2 v}{2v_1}\\
&\quad+\frac{1+7\ln v+\ln^2 v+6\ln v_1+8\ln^2 v_1}{2v}+\Delta c_1^{\mathrm{kq}},\\
\Delta c_1^{\mathrm{kq}} &= 4(1-\ln v-\ln^2 v)vv_1\tau(v), \qquad \tilde{c}_1^{\mathrm{kq}}=[4(\ln v-\ln v_1)-(3+4\ln v)vv_1]\tau(v),\\
c_2^{\mathrm{kq}} &= [-16\ln v+(-3+4\ln v)vv_1]\tau(v)+\Delta c_2^{\mathrm{kq}}, \qquad \Delta c_2^{\mathrm{kq}}=-4(1+2\ln v)vv_1\tau(v),\\
\tilde{c}_2^{\mathrm{kq}} &= (8-4v+4v^2)\tau(v), \qquad c_3^{\mathrm{kq}}=(-16+4v-4v^2)\tau(v)+\Delta c_3^{\mathrm{kq}}, \qquad \Delta c_3^{\mathrm{kq}}=-8vv_1\tau(v),\\
c_5^{\mathrm{kq}} &= \frac{-2(2-8v+6v^2-9v^3+v^4)}{v_1^2 v}-\frac{8(1-2v+2v^2)}{v_1 v w^2}-\frac{2(4-5v+5v^3)}{v_1^2 vw}-\frac{4(-1+4v-4v^2+5v^3)w}{v_1^2 v}\\
&\quad+\frac{4v_1 v}{X^3}+\frac{4v(-3+2v)}{X^2}-\frac{4v(-5+2v)}{v_1 X}+\frac{4v_1^2 v}{Y^3}-\frac{4v_1 v^2}{Y^2}+\frac{2v(3-6v+4v^2)}{Y}+\Delta c_5^{\mathrm{kq}},\\
\Delta c_5^{\mathrm{kq}} &= 4v-\frac{8vv_1^2}{Y^3}+\frac{8v^2 v_1}{Y^2}-\frac{4(3v-6v^2+4v^3)}{Y},\\
c_6^{\mathrm{kq}} &= \frac{2v(-5-5v+2v^2)}{v_1^2}+\frac{8(1-2v+2v^2)}{v_1 v w^2}-\frac{2(2-13v+16v^2-11v^3+2v^4)}{v_1^2 vw}-\frac{2(-9+v)v^2 w}{v_1^2},\\
c_7^{\mathrm{kq}} &= -6v-\frac{2(4-v+v^2)}{vw}+\frac{2v^2 w}{v_1}+\frac{8v_1^2 v}{Y^3}-\frac{8v_1 v^2}{Y^2}+\frac{4v(3-6v+4v^2)}{Y},\\
c_8^{\mathrm{kq}} &= \frac{2v(1+7v)}{v_1^2}-\frac{8(1-2v+2v^2)}{v_1 v w^2}+\frac{2(4-14v+17v^2-12v^3+v^4)}{v_1^2 vw}+\frac{4v(1-5v)w}{v_1^2},\\
c_9^{\mathrm{kq}} &= \frac{2v^2(7+v)}{v_1^2}-\frac{8(1-2v+2v^2)}{v_1 v w^2}-\frac{2(2-3v+2v^2+v^3+2v^4)}{v_1^2 vw}+\frac{2(-9+v)v^2 w}{v_1^2}+\frac{4v(2-2v+v^2)}{v_1 X},
\end{aligned}
$$

$$c_{10}^{\rm kq}=\frac{-2(2-8v+4v^2-9v^3+3v^4)}{v_1^2v}-\frac{8(1-2v+2v^2)}{v_1vw^2}+\frac{2(-4+2v+3v^2-8v^3+3v^4)}{v_1^2vw}$$
$$+\frac{2(2-8v+8v^2-11v^3+v^4)w}{v_1^2v}+\frac{4v_1v}{X^3}+\frac{4v(-3+2v)}{X^2}-\frac{4v(-3+v^2)}{v_1X}+\frac{4v_1^2v}{Y^3}-\frac{4v_1v^2}{Y^2}$$
$$+\frac{2v(3-6v+4v^2)}{Y}+\Delta c_{10}^{\rm kq},\quad \Delta c_{10}^{\rm kq}=\Delta c_5^{\rm kq},$$
$$c_{11}^{\rm kq}=-\frac{-10+31v-22v^2+7v^3+2v^4}{v_1^2v}-\frac{8}{w^2}-\frac{2(1-6v+6v^2)}{vw}-\frac{2(2-5v+v^2)(3-2v+v^2)w}{v_1^2v}-\frac{12v_1v}{X^3}$$
$$-\frac{2v(-12+7v)}{X^2}+\frac{v(-3-9v+10v^2)}{v_1X}-\frac{8v_1^2v}{Y^3}+\frac{4v_1v(-1+3v)}{Y^2}-\frac{v(-19+6v^2)}{Y}+\Delta c_{11}^{\rm kq},\quad \Delta c_{11}^{\rm kq}=\frac{1}{2}\Delta c_{10}^{\rm kq},$$
$$\tilde{c}_{11}^{\rm kq}=\frac{2(2-8v+10v^2-13v^3+v^4)}{v_1^2v}+\frac{8(1-2v+2v^2)}{v_1vw^2}-\frac{2(-5+12v-13v^2+2v^3)}{v_1^2w}$$
$$+\frac{4(-1+4v-4v^2+5v^3)w}{v_1^2v}-\frac{4v_1v}{X^3}-\frac{4v(-3+2v)}{X^2}+\frac{4v(-3+v^2)}{v_1X}-\frac{4v_1^2v}{Y^3}+\frac{4v_1v^2}{Y^2}-\frac{2v(3-6v+4v^2)}{Y},$$
$$c_{12}^{\rm kq}=6-16v+16v^2-\frac{8}{v_1}-\frac{8}{v},\quad c_{13}^{\rm kq}=10-2v+\frac{4}{v_1}-\frac{4}{v},\quad c_{14}^{\rm kq}=8+2v-\frac{4}{v_1}+\frac{4}{v}. \tag{A4}$$

4. Coefficient for the quark-loop contribution

$$c_1^{\rm ql}=\Delta c_1^{\rm ql},\qquad \Delta c_1^{\rm ql}=-\tfrac{4}{9}v(1-v). \tag{A5}$$

APPENDIX B: COEFFICIENTS FOR SUBPROCESS $q+\bar{q}\to c+\bar{c}$

In the following, we list the coefficients c_i needed for the calculation of the cross section for the inclusive production of charm in $q\bar{q}$ collisions. As before, the coefficients c_i are obtained from the cross sections of Ref. [7] by taking the limit $m\to 0$, whereas the subtraction terms Δc_i are deduced by a comparison with the results of Ref. [20]. The coefficients given in this appendix determine the cross section according to Eqs. (12) and (20) and using the color decomposition of Eq. (49). We start with the Abelian coefficients $c_i^{\rm cf}$.

1. $c_i^{\rm cf}$ coefficients

$$c_1^{\rm cf}=\frac{1}{3}\{24v\ln v_1+6(3-6v+2v^2)\ln^2v_1+5(-15+2\pi^2)(1-2v+2v^2)-24(3-6v+7v^2)\ln^2v+3[-11$$
$$+14v-6v^2+28(1-2v+2v^2)\ln v_1]\ln v\}+\Delta c_1^{\rm cf},$$
$$\Delta c_1^{\rm cf}=-4(-1+\ln v+\ln^2 v)\tau_q(v),\qquad \tilde{c}_1^{\rm cf}=(-9-8\ln v+4\ln v_1)\tau_q(v),$$
$$c_2^{\rm cf}=(-3-20\ln v+24\ln v_1)\tau_q(v)+\Delta c_2^{\rm cf},\qquad \Delta c_2^{\rm cf}=-4(1+2\ln v)\tau_q(v),\qquad \tilde{c}_2^{\rm cf}=-12\tau_q(v),$$
$$c_3^{\rm cf}=20\tau_q(v)+\Delta c_3^{\rm cf},\qquad \Delta c_3^{\rm cf}=-8\tau_q(v),$$
$$c_5^{\rm cf}=\frac{2(-1+34v-39v^2+8v^3)}{v_1}+\frac{4(1-2v+2v^2)}{w}-\frac{8v^2w}{v_1}+\frac{8v^3w^2}{v_1}-\frac{2v}{X}+\frac{4v_1^2v}{Y^3}-\frac{4v_1v^2}{Y^2}$$
$$-\frac{2(55v-74v^2+28v^3)}{Y}+\Delta c_5^{\rm cf},$$
$$\Delta c_5^{\rm cf}=4v-\frac{8vv_1^2}{Y^3}+\frac{8v^2v_1}{Y^2}-\frac{4(3v-6v^2+4v^3)}{Y},\qquad c_6^{\rm cf}=\frac{-4v(7-10v+4v^2)}{v_1}+\frac{8(2-v)v^2w}{v_1}-\frac{8v^3w^2}{v_1},$$
$$c_7^{\rm cf}=-20v+\frac{8vv_1^2}{Y^3}-\frac{8v^2v_1}{Y^2}+\frac{4(v-6v^2+4v^3)}{Y},$$
$$c_8^{\rm cf}=\frac{4v(-3+2v+2v^2)}{v_1}-\frac{8v^2w}{v_1}+\frac{8v^3w^2}{v_1}+\frac{16(5v-8v^2+4v^3)}{Y},$$

$$
\begin{aligned}
c_9^{\rm cf} &= 40v + \frac{4(1-2v+2v^2)}{w} + 8v^2 w - \frac{16(5v-8v^2+4v^3)}{Y},\\
c_{10}^{\rm cf} &= \frac{2(-1+22v-31v^2+12v^3)}{v_1} + \frac{4(1-2v+2v^2)}{w} - \frac{8(2-v)v^2 w}{v_1} + \frac{8v^3 w^2}{v_1} - \frac{2v}{X} + \frac{4vv_1^2}{Y^3} - \frac{4v^2 v_1}{Y^2}\\
&\quad + \frac{2(-15v+10v^2+4v^3)}{Y} + \Delta c_{10}^{\rm cf},\\
\Delta c_{10}^{\rm cf} &= \Delta c_5^{\rm cf}, \qquad c_{11}^{\rm cf} = \frac{-10+9v+3v^2}{v_1} + \frac{2}{w} + \frac{6v}{X} - \frac{8vv_1^2}{Y^3} - \frac{12(3v-4v^2+v^3)}{Y^2} - \frac{2(-11v+3v^3)}{Y} + \Delta c_{11}^{\rm cf},\\
\Delta c_{11}^{\rm cf} &= \frac{1}{2}\Delta c_{10}^{\rm cf},\\
\tilde{c}_{11}^{\rm cf} &= \frac{2(1-10v+15v^2-8v^3)}{v_1} - \frac{4(1-2v+2v^2)}{w} + \frac{8v^2 w}{v_1} - \frac{8v^3 w^2}{v_1} + \frac{2v}{X} - \frac{4v_1^2 v}{Y^3} + \frac{4v_1 v^2}{Y^2} - \frac{2(v-6v^2+4v^3)}{Y},\\
c_{12}^{\rm cf} &= 8(-1+2v+2v^2), \qquad c_{13}^{\rm cf} = -8(3-6v+8v^2), \qquad c_{14}^{\rm cf} = 16v_1^2.
\end{aligned}
\tag{B1}
$$

2. $c_i^{\rm ca}$ coefficients

$$
\begin{aligned}
c_1^{\rm ca} &= \frac{1}{9}\{-18v\ln v_1 + 9(-1+2v)\ln^2 v_1 - 2(-85+9\pi^2)(1-2v+2v^2) + 18(7-14v+16v^2)\ln^2 v\\
&\quad - 36[-1+v+(3-6v+6v^2)\ln v_1]\ln v\}, \qquad \tilde{c}_1^{\rm ca} = \frac{22}{3}\tau_q(v), \qquad c_2^{\rm ca} = 16\tau_q(v)\ln v, \qquad \tilde{c}_2^{\rm ca} = 0,\\
c_3^{\rm ca} &= 0, \qquad c_5^{\rm ca} = -4v(4+v) - 4v^2 w - \frac{4vv_1^2}{Y^3} + \frac{4(3v-5v^2+2v^3)}{Y^2} + \frac{2(19v-28v^2+12v^3)}{Y}, \qquad c_6^{\rm ca} = 4v,\\
c_7^{\rm ca} &= 18v - \frac{8vv_1^2}{Y^3} + \frac{8(3v-5v^2+2v^3)}{Y^2} - \frac{4(9v-12v^2+4v^3)}{Y},\\
c_8^{\rm ca} &= -2v(-7+2v) - 4v^2 w - \frac{2(17v-26v^2+12v^3)}{Y}, \qquad c_9^{\rm ca} = -4v(4+v) - 4v^2 w + \frac{2(17v-26v^2+12v^3)}{Y},\\
c_{10}^{\rm ca} &= -6v - \frac{4vv_1^2}{Y^3} + \frac{4(3v-5v^2+2v^3)}{Y^2} + \frac{4vv_1}{Y},\\
c_{11}^{\rm ca} &= 2(2-5v+2v^2) + 4v^2 w - \frac{2v}{X} + \frac{12vv_1^2}{Y^3} - \frac{12vv_1^2}{Y^2} + \frac{4(4v-7v^2+2v^3)}{Y},\\
\tilde{c}_{11}^{\rm ca} &= 4(-2+v)v + 4v^2 w + \frac{4vv_1^2}{Y^3} - \frac{4(3v-5v^2+2v^3)}{Y^2} + \frac{2(9v-12v^2+4v^3)}{Y}, \qquad c_{12}^{\rm ca} = -2+4v-16v^2,\\
c_{13}^{\rm ca} &= 4(3-6v+8v^2), \qquad c_{14}^{\rm ca} = -2+4v.
\end{aligned}
\tag{B2}
$$

3. Coefficient for the quark-loop contribution

$$
c_1^{\rm ql} = -\frac{20}{9}n_f\tau_q(v), \qquad \tilde{c}_1^{\rm ql} = -\frac{4}{3}n_f\tau_q(v). \tag{B3}
$$

APPENDIX C: COEFFICIENTS FOR SUBPROCESS $g + q \to c + \bar{c} + q$

This appendix contains the coefficients needed for the calculation of the cross section for $g + q \to c + \bar{c} + q$ with an observed charm quark in the final state according to Eq. (12). We note that there are no subtraction terms for the gq channel. In the following, again only nonzero coefficients are written down. According to the color decomposition defined in Eq. (65), we present the Abelian and non-Abelian coefficients $c_i^{\rm cf}$ and $c_i^{\rm ca}$ separately.

1. $c_i^{\rm cf}$ coefficients

$$
\begin{aligned}
c_5^{\rm cf} &= \frac{-2(1-2v+6v^2-5v^3+2v^4)}{v_1^2}+\frac{2(1-2v+4v^2-3v^3+v^4)}{v_1^2 w}+\frac{2(1-2v+6v^2-5v^3+2v^4)w}{v_1^2}\\
&\quad+\frac{v}{2X^2}+\frac{-3v+v^2}{2v_1X}-\frac{v_1 v}{2Y^2}+\frac{3v-2v^2}{2Y}, \quad c_6^{\rm cf}=\frac{2v(1+v^2)}{v_1^2}+\frac{-1-v^2}{v_1^2 w}-\frac{4v^3 w}{v_1^2},\\
c_7^{\rm cf} &= \frac{-2v}{v_1}+\frac{4v^2 w}{v_1}-\frac{vv_1}{Y^2}+\frac{3v-2v^2}{Y}, \quad c_8^{\rm cf}=\frac{-2v(3-3v+2v^2)}{v_1^2}+\frac{1+v^2}{v_1^2 w}+\frac{4v(2-3v+2v^2)w}{v_1^2},\\
c_9^{\rm cf} &= \frac{-4(1-2v+5v^2-4v^3+v^4)}{v_1^2}+\frac{2(1-2v+4v^2-3v^3+v^4)}{v_1^2 w}+\frac{4v^2(5-5v+v^2)w}{v_1^2}-\frac{16v^2w^2}{v_1},\\
c_{10}^{\rm cf} &= \frac{-2(-1+2v-v^2+2v^4)}{v_1^2}+\frac{2(1-2v+4v^2-3v^3+v^4)}{v_1^2 w}+\frac{2(1-2v-4v^2+5v^3+2v^4)w}{v_1^2}+\frac{16v^2w^2}{v_1}\\
&\quad+\frac{v}{2X^2}+\frac{-3v+v^2}{2v_1X}-\frac{v_1 v}{2Y^2}+\frac{3v-2v^2}{2Y},\\
c_{11}^{\rm cf} &= \frac{2v^2(4-5v+2v^2)}{v_1^2}+\frac{1+2v-2v^2}{2w}-\frac{(-2+4v+7v^2-11v^3+4v^4)w}{v_1^2}-\frac{v}{2X^2}+\frac{5v-4v^2}{2v_1X}+\frac{v_1 v}{Y^2}+\frac{-8v+3v^2}{2Y},\\
\tilde{c}_{11}^{\rm cf} &= \frac{2(1-2v+6v^2-5v^3+2v^4)}{v_1^2}-\frac{2(1-2v+4v^2-3v^3+v^4)}{v_1^2 w}-\frac{2(1-2v+6v^2-5v^3+2v^4)w}{v_1^2}\\
&\quad-\frac{v}{2X^2}+\frac{3v-v^2}{2v_1X}+\frac{v_1 v}{2Y^2}+\frac{-3v+2v^2}{2Y}.
\end{aligned}
\tag{C1}
$$

We have checked that the following relations between these results for the C_F part and the coefficients for the subprocess $\gamma + q \to c + \bar{c} + q$ in Ref. [17] are satisfied, if the normalization factors $C(s)$, $C_q(s)$, $C_{cq}(s)$ and C_F are replaced by unity: $c_i^{\rm cf} = c_i^{Q_1} + c_i^{Q_2} - 2c_i^{Q_3}$. Furthermore, our results in Appendix D 1 fulfill the relations $c_i^{{\rm cf},\bar{c}-c} = 4c_i^{Q_3}$ and $c_i^{\rm cf} + c_i^{{\rm cf},\bar{c}-c}/2 = c_i^{Q_1} + c_i^{Q_2}$.

The decomposition of the form $e_c^2 Q_1 + e_q^2 Q_2 - e_c e_q Q_3$ for $\gamma + q \to Q$ turns into one of the form $Q_1 + Q_2 - 2Q_3$ for $g + q \to Q$. The interference part Q_3 is antisymmetric and changes sign in the analogous subprocesses with an antiquark $\bar{q}$, i.e., we have $e_c^2 Q_1 + e_{\bar{q}}^2 Q_2 + e_c e_q Q_3$ for $\gamma + \bar{q} \to Q$ and $Q_1 + Q_2 + 2Q_3$ for $g + \bar{q} \to Q$.

2. $c_i^{\rm ca}$ coefficients

$$
\begin{aligned}
c_5^{\rm ca} &= -\frac{v^2(2-2v+v^2)}{v_1^2}+\frac{4v^2(1-v+v^2)w}{v_1^2}-\frac{6v^4w^2}{v_1^2}+\frac{4v^4w^3}{v_1^2}-\frac{v}{2X}+\frac{v}{2Y},\\
c_6^{\rm ca} &= \frac{v(1+v)}{v_1^2}-\frac{v^2(5-v+2v^2)w}{v_1^2}+\frac{4v^3(1+v)w^2}{v_1^2}-\frac{4v^4w^3}{v_1^2},\\
c_7^{\rm ca} &= -v-\frac{v^2 w}{v_1}+\frac{v}{Y}, \quad c_8^{\rm ca}=-\frac{v(-1+4v-3v^2+v^3)}{v_1^2}+\frac{2v(-1+4v-3v^2+2v^3)w}{v_1^2}-\frac{6v^4w^2}{v_1^2}+\frac{4v^4w^3}{v_1^2},\\
c_9^{\rm ca} &= -\frac{-1+2v-v^2+v^4}{v_1^2}+\frac{v^2(-1+v+2v^2)w}{v_1^2}-\frac{2v^2(-2+2v+v^2)w^2}{v_1^2},\\
c_{10}^{\rm ca} &= -\frac{1-v+5v^2}{v_1}+\frac{v^2(11-11v+2v^2)w}{v_1^2}-\frac{4v^2(1-v+v^2)w^2}{v_1^2}+\frac{4v^4w^3}{v_1^2}-\frac{v}{2X}+\frac{v}{2Y},\\
c_{11}^{\rm ca} &= 1+v^2+\frac{2(-1+v+v^3)w}{v_1}+\frac{2v^3(-1+2v)w^2}{v_1^2}-\frac{2v^4w^3}{v_1^2}-\frac{v}{X}+\frac{v}{2Y},\\
\tilde{c}_{11}^{\rm ca} &= \frac{v^2(2-2v+v^2)}{v_1^2}-\frac{4v^2(1-v+v^2)w}{v_1^2}+\frac{6v^4w^2}{v_1^2}-\frac{4v^4w^3}{v_1^2}+\frac{v}{2X}-\frac{v}{2Y}.
\end{aligned}
\tag{C2}
$$

APPENDIX D: COEFFICIENTS FOR SUBPROCESS $g + \bar{q} \to c + \bar{c} + \bar{q}$

The cross sections for the subprocesses $g + q \to c + \bar{c} + q$ and $g + \bar{q} \to c + \bar{c} + \bar{q}$, where the quark in the initial state is replaced by an antiquark, are related, but not identical. The differences between the corresponding coefficients, $c_i^{\bar{c}-c}$, will be presented below. They have to be combined with the coefficients for $g + q \to c + \bar{c} + q$ given in Appendix C to give those for $g + \bar{q} \to c + \bar{c} + \bar{q}$, according to $c_i(g + \bar{q} \to c + \bar{c} + \bar{q}) = c_i(g + q \to c + \bar{c} + q) + c_i^{\bar{c}-c}$, to be inserted in Eqs. (12) and (65). Again, there are no subtraction terms, and we present only the nonzero coefficients. Note, in particular, that for both color factors $c_{1-5}^{\bar{c}-c}$ and $c_{12-14}^{\bar{c}-c}$ are zero.

1. c_i^{cf} coefficients

$$
\begin{aligned}
&c_6^{\mathrm{cf},\bar{c}-c} = \frac{4v^2}{v_1} - \frac{8v^2w}{v_1}, \qquad c_7^{\mathrm{cf},\bar{c}-c} = c_6^{\mathrm{cf},\bar{c}-c}, \qquad c_8^{\mathrm{cf},\bar{c}-c} = 8v - 16vw,\\
&c_9^{\mathrm{cf},\bar{c}-c} = \frac{4(2-2v+3v^2)}{v_1} - \frac{24v^2w}{v_1} + \frac{32v^2w^2}{v_1}, \qquad c_{10}^{\mathrm{cf},\bar{c}-c} = \frac{-4(2-2v+5v^2)}{v_1} + \frac{40v^2w}{v_1} - \frac{32v^2w^2}{v_1},\\
&c_{11}^{\mathrm{cf},\bar{c}-c} = 8 - 16w - \frac{4v}{X} + \frac{4v}{Y}.
\end{aligned}
\tag{D1}
$$

2. c_i^{ca} coefficients

$$
\begin{aligned}
&c_6^{\mathrm{ca},\bar{c}-c} = \frac{-3v^2}{2v_1} + \frac{3v^2w}{v_1}, \qquad c_7^{\mathrm{ca},\bar{c}-c} = c_6^{\mathrm{ca},\bar{c}-c}, \qquad c_8^{\mathrm{ca},\bar{c}-c} = -3v + 6vw,\\
&c_9^{\mathrm{ca},\bar{c}-c} = \frac{-3(2-2v+3v^2)}{2v_1} + \frac{9v^2w}{v_1} - \frac{12v^2w^2}{v_1}, \qquad c_{10}^{\mathrm{ca},\bar{c}-c} = \frac{3(2-2v+5v^2)}{2v_1} - \frac{15v^2w}{v_1} + \frac{12v^2w^2}{v_1},\\
&c_{11}^{\mathrm{ca},\bar{c}-c} = -3 + 6w + \frac{3v}{2X} - \frac{3v}{2Y}.
\end{aligned}
\tag{D2}
$$

[1] CDF Collaboration, D. Acosta *et al.*, Phys. Rev. Lett. **91**, 241804 (2003).
[2] M. Cacciari and M. Greco, Nucl. Phys. **B421**, 530 (1994).
[3] J. Binnewies, B. A. Kniehl, and G. Kramer, Phys. Rev. D **58**, 014014 (1998).
[4] P. Nason, S. Dawson, and R. K. Ellis, Nucl. Phys. **B303**, 607 (1988); **B327**, 49 (1988); **B335**, 260(E) (1990).
[5] W. Beenakker, H. Kuijf, W. L. van Neerven, and J. Smith, Phys. Rev. D **40**, 54 (1989).
[6] W. Beenakker, W. L. van Neerven, R. Meng, G. A. Schuler, and J. Smith, Nucl. Phys. **B351**, 507 (1991).
[7] I. Bojak and M. Stratmann, Phys. Rev. D **67**, 034010 (2003).
[8] M. A. G. Aivazis, J. C. Collins, F. I. Olness, and W.-K. Tung, Phys. Rev. D **50**, 3102 (1994).
[9] F. I. Olness, R. J. Scalise, and W.-K. Tung, Phys. Rev. D **59**, 014506 (1999).
[10] M. Cacciari, M. Greco, and P. Nason, J. High Energy Phys. 05 (1998) 007.
[11] M. Cacciari and P. Nason, J. High Energy Phys. 09 (2003) 006.
[12] W. K. Tung, S. Kretzer, and C. Schmidt, J. Phys. G **28**, 983 (2002), and references therein.
[13] V. N. Gribov and L. N. Lipatov, Yad. Fiz. **15**, 781 (1972) [Sov. J. Nucl. Phys. **15**, 438 (1972)]; G. Altarelli and G. Parisi, Nucl. Phys. **B126**, 298 (1977); Yu. L. Dokshitser, Zh. Eksp. Teor. Fiz. **73**, 1216 (1977) [Sov. Phys. JETP **46**, 641 (1977)].
[14] J. C. Collins, Phys. Rev. D **58**, 094002 (1998).
[15] S. Kretzer, H. L. Lai, F. I. Olness, and W. K. Tung, Phys. Rev. D **69**, 114005 (2004).
[16] G. Kramer and H. Spiesberger, Eur. Phys. J. C **22**, 289 (2001).
[17] G. Kramer and H. Spiesberger, Eur. Phys. J. C **28**, 495 (2003).
[18] G. Kramer and H. Spiesberger, Report No. DESY 04-196, MZ-TH/03-18 (hep-ph/0311062).
[19] B. A. Kniehl and G. Kramer (to be published).
[20] F. Aversa, P. Chiappetta, M. Greco, and J. Ph. Guillet, Phys. Lett. B **210**, 225 (1988); **211**, 465 (1988); Nucl. Phys. **B327**, 105 (1989).
[21] B. A. Kniehl and G. Kramer, Z. Phys. C **62**, 53 (1994); J. Binnewies, B. A. Kniehl, and G. Kramer, Z. Phys. C **76**, 677 (1997); B. A. Kniehl, G. Kramer, and M. Spira, Z. Phys. C **76**, 689 (1997).

[22] I. Bojak and M. Stratmann, Phys. Lett. B **433**, 411 (1998); Nucl. Phys. **B540**, 345 (1999); **B569**, 694(E) (2000); I. Bojak, Ph.D. thesis, University of Dortmund, 2000, Report No. DO-TH 2000/09 (hep-ph/0005120).

[23] It should be noted that there is no such contribution in the massless limit of the calculation of Ref. [5], i.e., $c_1^{\mathrm{ql}} = \Delta c_1^{\mathrm{ql}} = 0$. On the other hand, we found nonzero coefficients c_1^{ql} and Δc_1^{ql} in the massless limit of Ref. [7] listed in Appendix A 4, which are numerically irrelevant, however.

[24] B. Mele and P. Nason, Nucl. Phys. **B361**, 626 (1991); J. P. Ma, Nucl. Phys. **B506**, 329 (1997); S. Kretzer and I. Schienbein, Phys. Rev. D **58**, 094035 (1998); **59**, 054004 (1999); K. Melnikov and A. Mitov, Phys. Rev. D **70**, 034027 (2004); A. Mitov, Report No. UH-511-1059-2004 (hep-ph/0410205).

[25] M. Krämer, F. I. Olness, and D. E. Soper, Phys. Rev. D **62**, 096007 (2000).

[26] Z. Merebashvili, A. P. Contogouris, and G. Grispos, Phys. Rev. D **62**, 114509 (2000); **69**, 019901(E) (2004).

[27] L. E. Gordon, Phys. Rev. D **50**, 6753 (1994).

[28] P. Aurenche, A. Douiri, R. Baier, M. Fontannaz, and D. Schiff, Phys. Lett. **135B**, 164 (1984); P. Aurenche, R. Baier, A. Douiri, M. Fontannaz, and D. Schiff, Nucl. Phys. **B286**, 553 (1987).

[29] CTEQ Collaboration, J. Pumplin *et al.*, J. High Energy Phys. 07 (2002) 012; CTEQ Collaboration, D. Stump *et al.*, J. High Energy Phys. 10 (2003) 046.

[30] B. Kamal, Z. Merebashvili, and A. P. Contogouris, Phys. Rev. D **51**, 4808 (1995); **55**, 3229(E) (1997).